ACS Infectious Diseases

pubs.acs.org/journal/aidcbc

Article

Trypanosoma cruzi Malic Enzyme Is the Target for Sulfonamide Hits from the GSK Chagas Box

Gustavo F. Mercaldi,[‖] Amanda G. Eufrásio,[‖] Americo T. Ranzani, Jessica do Nascimento Faria, Sabrina G. R. Mota, Michelle Fagundes, Marjorie Bruder,[*] and Artur T. Cordeiro[*]

Cite This: https://doi.org/10.1021/acsinfecdis.1c00231

Read Online

ACCESS | Metrics & More | Article Recommendations | Supporting Information

ABSTRACT: Chagas disease, an infectious condition caused by *Trypanosoma cruzi*, lacks treatment with drugs with desired efficacy and safety profiles. To address this unmet medical need, a set of trypanocidal compounds were identified through a large multicenter phenotypic-screening initiative and assembled in the GSK Chagas Box. In the present work, we report the screening of the Chagas Box against *T. cruzi* malic enzymes (MEs) and the identification of three potent inhibitors of its cytosolic isoform (TcMEc). One of these compounds, TCMDC-143108 (**1**), came out as a nanomolar inhibitor of TcMEc, and 14 new derivatives were synthesized and tested for target inhibition and efficacy against the parasite. Moreover, we determined the crystallographic structures of TcMEc in complex with TCMDC-143108 (**1**) and six derivatives, revealing the allosteric inhibition site and the determinants of specificity. Our findings connect phenotypic hits from the Chagas Box to a relevant metabolic target in the parasite, providing data to foster new structure−activity guided hit optimization initiatives.

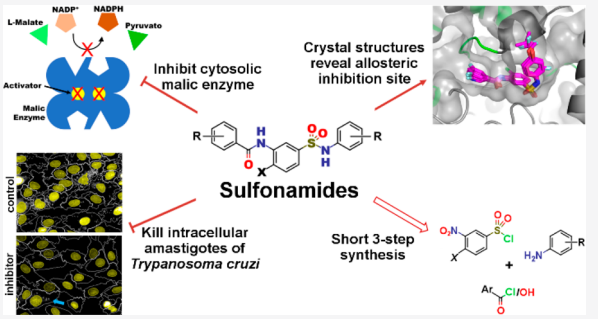

KEYWORDS: *Trypanosoma cruzi, malic enzyme, sulfonamides, GSK Chagas Box, Tres Cantos anti-kinetoplastids set, target-inhibitor structure*

INTRODUCTION

Malic enzymes (MEs) are preserved in several living organisms, from fungi to mammals, and catalyze the oxidative decarboxylation of malate to pyruvate with the concomitant reduction of NAD^+ or $NADP^+$. In humans, there are three ME isoforms: the cytosolic $NADP^+$-dependent ME1 (EC 1.1.1.40),[1] the mitochondrial $NADP^+$-dependent ME3 (EC 1.1.1.40),[2] and the mitochondrial ME2 (EC 1.1.1.38), which can use both NAD^+ and $NADP^+$ as the cofactor, but with preference for the first one[3]. Moreover, ME2 is the only isoform in humans which is allosterically activated by fumarate and inhibited by ATP. Allosteric activation is not an exclusive property of the mammalian ME2, as similar enzymatic behavior is also observed in bacterial,[4] protozoan,[5,6] roundworm,[7] and plant[8] homologous enzymes.

In general, the biological relevance of ME is associated with NADPH production and its essential role in biosynthetic pathways and neutralization of reactive oxygen species. Interfering with ME enzymatic activity has been considered an attractive strategy toward drug discovery against different diseases. In cancer, pancreatic adenocarcinoma cells recurrently have the ME2 gene deleted because of passenger deletions of other tumor suppressor genes. ME3 depletion in ME2-null pancreatic adenocarcinoma cells brakes redundancy for NADPH production in mitochondria and induces selective cell dead.[9] In bacteria and protozoan parasites, particularities in structure and allosteric regulation suggest that ME might be explored for the development of new antimicrobial agents. While the human mitochondrial ME2 is activated by fumarate and inhibited by ATP,[10] in *Trypanosoma cruzi*[5] and *Leishmania mexicana*[6] the cytosolic isoform is allosterically activated by L-aspartate. Moreover, these protozoan parasites have only two ME isoforms, one in the cytosol (MEc) and another in the mitochondrion (MEm), and both are $NADP^+$-dependent.

Crystal structures are presently available for ME1[11,12] and ME2[13−15] but not for ME3. Human MEs are all tetrameric proteins, and monomers are formed by four domains, named A−D, from the N- to C-terminal. The characterization of ME2 complexes with its usual ligands allowed Chang and Tong to propose a molecular mechanism for its allosteric activation by fumarate and inhibition by ATP.[16] According to the proposed model, the tetramer may exist in an equilibrium among four distinct forms (open I, open II, closed I, and closed II), which

Received: April 26, 2021

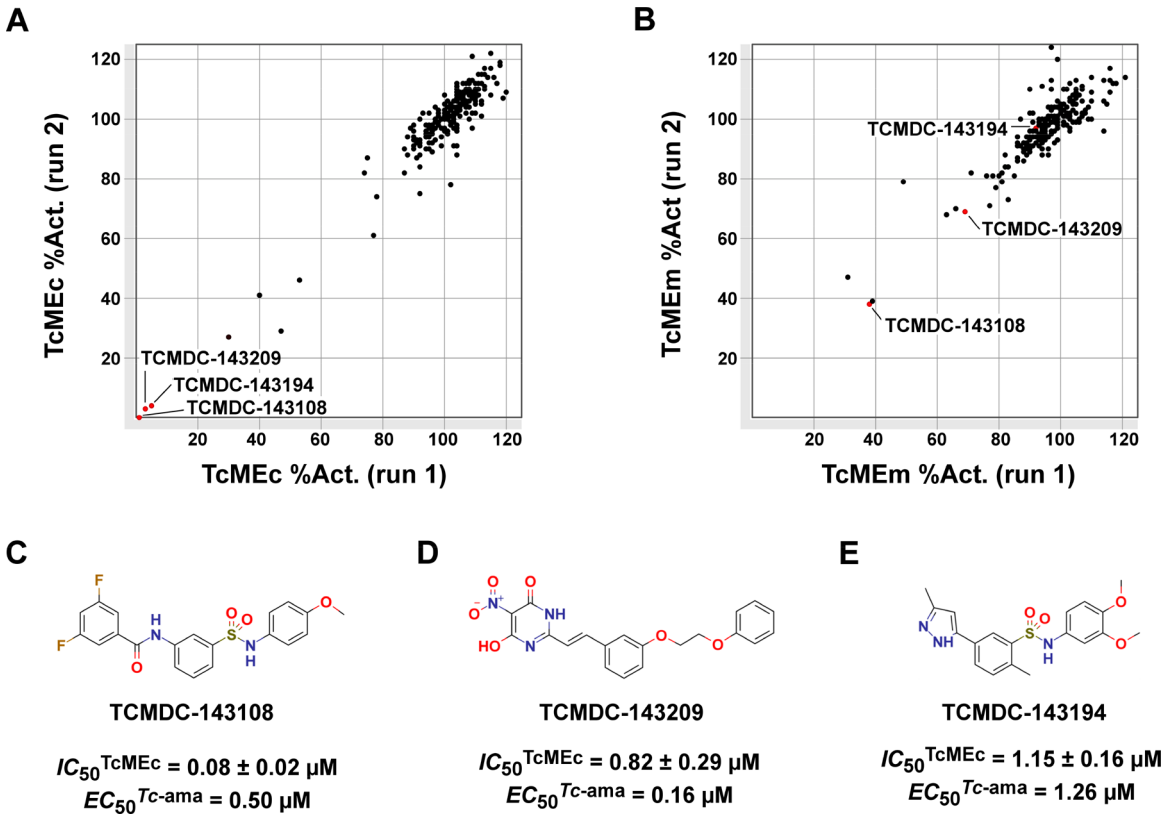

Figure 1. Screening of the Chagas Box trypanocidal compounds reveals potent inhibitors of the parasitic cytosolic malic enzyme. 218 Compounds from Chagas Box were tested at 5 μM in duplicate against the cytosolic (A) and mitocondrial (B) isoforms of *T. cruzi* malic enzymes (TcMEc and TcMEm, respectively). Compounds TCMDC-143108 (**1**) (C), TCMDC-143209 (**2**) (D), and TCMDC-143194 (**3**) (E) had their activity confirmed and IC_{50} values determined in dose−response assays performed with resupplied, ready to use sample plates. Percentage of activity (% Act) was obtained by normalization of data using positive and negative controls. *EC_{50} values were obtained from previously reported studies.[18]

can be interconverted through small rearrangements of its domains. The reaction is catalyzed by the approximation of malate and $NADP^+$ binding domains (active site closure), which can happen in the presence or absence of fumarate. The binding of fumarate to the ME2 dimeric interface facilitates domain rearrangement, which promotes the transition from state I to II and favors catalysis.

Our initial hypothesis was that structural and functional differences between human and protozoan parasites could be explored for the identification of selective inhibitors of MEs from *T. cruzi*, the causative agent of Chagas disease. In our previous work, we had identified sulfonamides as nanomolar inhibitors, with high selectivity toward the cytosolic *T. cruzi* ME isoform (TcMEc).[17] Moreover, a single concentration screening for TcMEc inhibitors against the Chagas Box, a collection of 222 hit compounds organized by GSK after a phenotypic high throughput screen of 1.8 million compounds,[18] indicated the presence of new TcMEc inhibitors in this collection of anti-*T. cruzi* hits.

In the present work, we report the results from the screening of the Chagas Box against *T. cruzi* cytosolic and mitochondrial ME isoforms and the identification of three compounds with remarkable activity over TcMEc. In addition, we describe the synthesis of TCMDC-143108 (**1**), the most potent TcMEc inhibitor, as well as of 14 new derivatives of this molecule. This new series was assayed for TcMEc inhibition as well as for their efficacy through an image-based assay against *T. cruzi* intracellular forms infecting H9c2 rat cardiomyocytes. Moreover, we determined crystallographic structures for TcMEc in its ligand free form and in complex with hit compound **1** and six analogues. To the best of our knowledge, TCMDC-143108 (**1**) is the first hit from the GSK Chagas Box to be reported as a *T. cruzi* metabolic enzyme inhibitor and to appear in a crystallographic complex with its target. This data can now be explored for structure-based hit-to-lead optimization of the trypanocidal compounds.

RESULTS AND DISCUSSION

In recent decades, there has been a growing trend for the use of phenotypic-based screening to identify bioactive molecules, particularly in drug discovery programs for infectious diseases.[19−23] As such, this strategy has been employed for the identification of compounds active against protozoan parasites.[18,19,21] Although successful for identifying novel hits with distinct chemical scaffolds, an intrinsic drawback of this approach is the lack of information about the primary mode of action of the selected molecules, creating the need for target deconvolution or identification.[22] Aiming to help filling this gap, we decided to test Chagas Box compounds[18] against the *T. cruzi* malic enzyme, a key enzyme in energetic metabolism and a promising target for Chagas disease under investigation in our group.[17,24,25]

***T. cruzi* Malic Enzymes are Inhibited by Small Molecules from the Chagas Box.** Some of the previously reported ME inhibitors[17] share common structural features with the compounds present in the Chagas Box,[18] which prompted us to screen this collection for inhibitors of cytosolic and mitochondrial *T. cruzi* ME isoforms (Figure 1A and B).

https://doi.org/10.1021/acsinfecdis.1c00231
ACS Infect. Dis. XXXX, XXX, XXX−XXX

Table 1. Data Collection and Refinement Statistics of Structures of TcΔMEc in Complex with Inhibitors

ligand	1	31	41	40	33	39	34	-
data collection statistics								
resolution (Å)	47.50−2.14 (2.20−2.14)	47.69−1.88 (1.92−1.88)	47.69−1.70 (1,73−1.70)	47.29−2.10 (2.16−2.10)	47.4−1.9 (1.94−1.90)	47.40−1.78 (1.82−1.78)	47.43−1.95 (2.00−1.95)	29.22−1.55 (1.58−1.55)
space group	$P4_32_12$	$P4_32_12$	$P4_32_12$	$P4_32_12$	$P4_32_12$	$P4_32_12$	$P4_32_12$	$P4_32_12$
cell parameters								
$a = b$; c (Å)	73.5; 233.7	73.8; 234.5	73.8; 234.5	73.2; 233.1	73.4; 233.6	73.4; 233.2	73.4; 233.8	73.3; 233.8
$\alpha = \beta = \gamma$ (deg)	90	90	90	90	90	90	90	90
X-ray source	W01B-MX2 (LNLS)	W01B-MX2 (LNLS)	W01B-MX2 (LNLS)	W01B-MX2 (LNLS)	W01B-MX2 (LNLS)	W01B-MX2 (LNLS)	W01B-MX2 (LNLS)	I03 (diamond)
wavelength (Å)	1.46	1.46	1.46	1.46	1.46	1.46	1.46	0.98
no. of unique reflections	36 499 (2879)	53 637 (3114)	72 505 (3730)	35 984 (2272)	50 906 (3215)	61 897 (3463)	47 202 (2994)	93 475 (4549)
R_{meas} [a]	0.14 (1.18)	0.09 (1.03)	0.06 (0.64)	0.08 (0.58)	0.09 (0.83)	0.06 (0.95)	0.10 (0.70)	0.09 (1.68)
completeness (%)	99.9 (98.8)	99.4 (91.9)	99.9 (99.0)	95.1 (75.0)	99.3 (98.6)	99.7 (99.9)	99.0 (90.8)	100.0 (100.0)
$\langle I/\sigma(I)\rangle$	13.0 (1.3)	19.4 (1.9)	24.6 (2.7)	14.4 (2.4)	12.6 (1.6)	20.1 (1.9)	9.2 (1.1)	17.9 (1.7)
$CC_{1/2}$								0.999 (0.613)
multiplicity	11.1 (4.8)	11.1 (7.5)	11.7 (6.5)	6.1 (4.7)	6.0 (3.8)	6.0 (5.5)	5.2 (2.6)	14.4 (12.5)
Wilson B factor (Å^2)	35.7	22.2	18.1	32.0	24.2	23.4	31.6	19.7
refinement statistics								
R_{work}	0.21 (0.34)	0.19 (0.30)	0.17 (0.23)	0.18 (0.26)	0.18 (0.28)	0.18 (0.27)	0.19 (0.33)	0.18 (0.27)
R_{free}	0.24 (0.39)	0.22 (0.33)	0.20 (0.24)	0.20 (0.29)	0.20 (0.28)	0.20 (0.31)	0.21 (0.33)	0.20 (0.29)
amino acid residues	545	544	543	540	544	542	544	547
heteroatoms (n)	61	58	54	48	46	47	47	28
solvent (n)	74	337	525	226	318	332	269	343
avg B factor (Å^2)								
protein	42.8	29.3	23.3	38.9	31.5	29.7	35.4	24.1
ligand	77.7	38.8	19.8	34.8	32.4	26.7	43.7	
citrate	60.0	52.6	39.4					30.6
HEPES	51.4	31.7	26.7	43.6	35.5	33.2	40.2	29.4
water	37.3	33.1	31.4	40.1	34.1	33.4	36.4	29.7
RSCC/RSR								
ligand	0.92/0.20	0.95/0.12	0.98/0.06	0.98/0.08	0.98/0.08	0.98/0.07	0.97/0.11	
citrate	0.92/0.13	0.93/0.13	0.90/0.15					0.94/0.10
HEPES	0.93/0.10	0.95/0.09	0.94/0.09	0.96/0.09	0.95/0.09	0.95/0.09	0.96/0.08	0.94/0.07
validation								
Ramachandran								
favored	529 (97%)	529 (97%)	530 (98%)	524 (98%)	535 (98%)	522 (97%)	524 (97%)	534 (98%)
allowed	14 (3%)	12 (2%)	10 (2%)	10 (2%)	9 (2%)	14 (3%)	17 (3%)	10 (2%)
PDB ID	6W29	6W2N	6W49	6W53	6W56	6W57	6W59	7MF4

[a] $R_{meas} = \Sigma_{hkl}[N/(N-1)]^{1/2}\ \Sigma_i|I_i(hkl) - \langle I(hkl)\rangle|/\Sigma_{hkl}\Sigma_i I_i(hkl)$.

Among the trypanocidal compounds tested, three molecules (TCMDC-143108 (**1**), TCMDC-143209 (**2**), and TCMDC-143194 (**3**)) completely abolished TcMEc activity while only showing a weak effect over TcMEm at the concentration of 5 μM. In addition, these molecules were shown to be potent inhibitors of TcMEc in confirmatory variable concentration assays (Figure 1C−E). Notably, the sulfonamide **1** which is known to be active against *T. cruzi* intracellular amastigotes with an EC_{50} of 0.5 μM,[18] showed a remarkable inhibitory activity over TcMEc with an IC_{50} value of 80 nM.

Although we have previously reported potent TcMEc inhibitors with a diaryl-sulfonamide scaffold, these molecules showed weak or no effects over *T. cruzi* epimastigote growth.[17] Further assays with a subset of 64 of the previously identified molecules, having TcMEc IC_{50} values between 6.2 μM and 3.2 nM, showed that these molecules were not effective against intracellular amastigote forms infecting H9c2 cardiomyocytes (Supporting Information, Table S1). Thus, compound **1** is a new TcMEc inhibitor with a better in vitro activity profile, showing trypanocidal activity in distinct assay formats, low host-cell toxicity, and no activity over CYP51.[18]

A Crystal Structure of the TcMEc:Inhibitor Complex Reveals the Target Allosteric Site. To establish the determinants of binding and mechanism of inhibition of **1**, we prepared sufficient quantities thereof (please refer to the synthesis section for further details) in order to solve the crystal structure of TcMEc in complex with the inhibitor (Table 1). Bipyramidal crystals of the truncated TcMEc (TcΔMEc, residues Q12-L565), with dimensions of up to 0.4 mm, were obtained after 1−2 weeks incubation at 18 °C. These crystals were soaked with **1** for 24 h before collection of diffraction data using synchrotron radiation. TcΔMEc crystals

https://doi.org/10.1021/acsinfecdis.1c00231
ACS Infect. Dis. XXXX, XXX, XXX−XXX

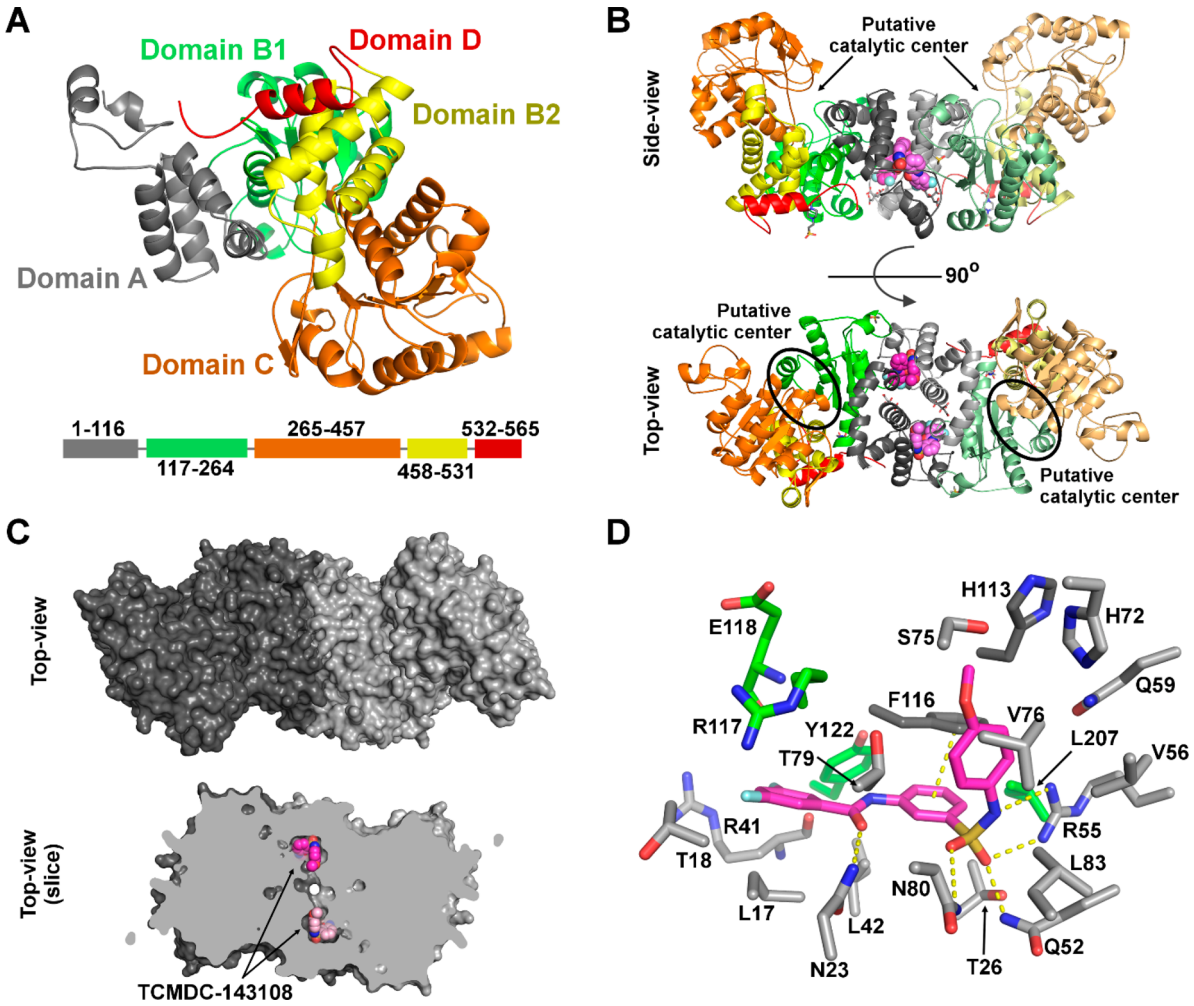

Figure 2. Crystal structure of *T. cruzi* malic enzyme (TcMEc) in complex with the trypanocidal compound TCMDC-143108 (**1**). (A) Overall fold of TcMEc showing domain organization. (B) TcMEc dimer built by crystallographic symmetry operations, showing symmetry mate macromolecule and sulfonamide inhibitor (**1**) in light colors and with the location of the putative catalytic center indicated. (C) Inspection of the solvent accessible surface of TcMEc dimer shows that the inhibitors are buried in a pocket found at the dimer interface, as revealed by the sliced view in the middle of the macromolecule. (D) TcMEc residues forming the allosteric binding site of **1** (sticks with magenta carbons). Side chains are represented as sticks, and carbon atoms are colored according to domains organization.

belonged to the tetragonal system and molecular replacement placed one polypeptide chain in the assimetric unit. In the refined structure (PDB 6W29), each polypeptide chain contained one bound molecule of **1**, in addition to highly ordered HEPES and citrate molecules that were present in the crystallization solution.

The TcMEc protomer has an overall fold that resembles the structures of MEs found in eukaryotes, like humans,[11,13−15,26,27] pigeons,[12] plants,[28] and nematodes,[29,30] and some prokaryotes like *Mycobacterium tuberculosis*, all organized in four domains named A to D (Figure 2A).

Contrary to the majority of the eukaryotic large unit MEs, TcMEc does not have N- nor C-terminal extensions that are known to stabilize the tetrameric form of the enzyme[14,16,28,31] (Figure S1). Further, TcMEc showed an estimated molecular mass equivalent to a dimer in size exclusion chromatography (SEC) experiments (Figure S2), which is in agreement with previous studies.[32,33] The TcMEc biological unit, which corresponds to the dimer, can be built by crystallographic symmetry operations (e.g., symmetry mates X, Y, Z and Y, X, −Z). The dimeric interface is formed exclusively by residues from domains A and B, it buries an area of 4580 Å^2,[34] and two symmetry related inhibitor (**1**) molecules are bound to separated but identical sites (Figure 2B).

Inspection of the solvent accessible surface showed that the ligand's binding site is completely buried into the dimer interface, without evident access to the solvent and distant from the substrate or cofactor binding sites, as described for other MEs[12−16,28,29,31] (Figure 2C). Consequently, local structural adjustments would be required for the ligand to access its binding pocket. Notably, in both human mitochondrial and *Ascaris suum* MEs, the site of the allosteric activator fumarate has also been mapped at the dimer interface.[15,16,26,30] Comparison of the TcMEc structure with that of the human mitochondrial isoform (HsME2, PDB 1GZ3) shows that ligand **1** superposes with fumarate (Figure S3). This observation indicates that the sulfonamide inhibitor (**1**) could be binding to the allosteric site in TcMEc, which is activated by aspartate.[5] Previous studies with the mitochondrial isoform of the human ME (HsME2) have shown that the enzyme could be allosterically inhibited by fumarate analogues or by embonic acid.[35,36] Despite crystallographic structures for HsME2 in complex with allosteric inhibitors not yet being available, site directed mutagenesis was used to demonstrate

https://doi.org/10.1021/acsinfecdis.1c00231
ACS Infect. Dis. XXXX, XXX, XXX−XXX

Scheme 1. Synthesis of Sulfonamides 1 and 30−43

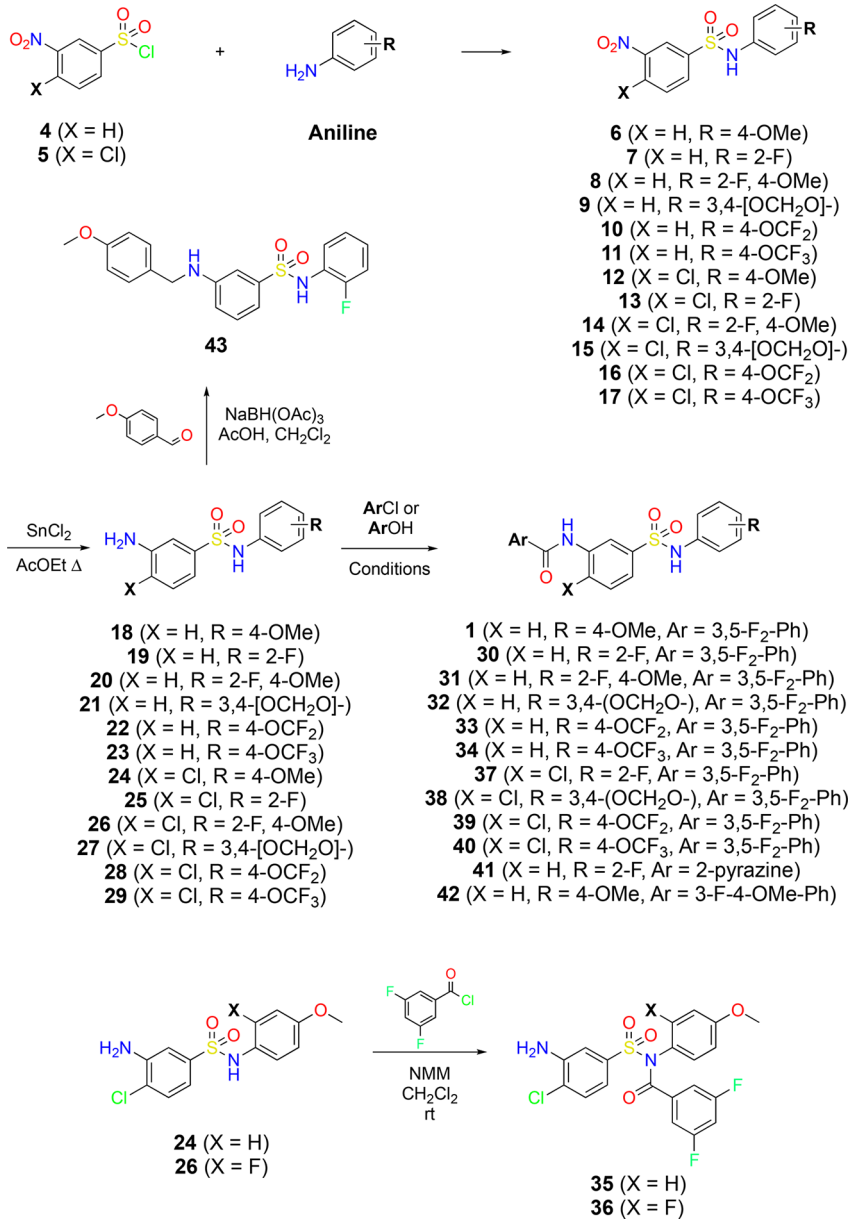

that modifications in the allosteric site causes a desensitization of the enzyme toward fumarate and negatively impact the binding affinity of embonic acid.[35,36] For instance, mutations of HsME2 residues R67 and R91 generate mutants insensitive to embonic acid inhibition and also fumarate activation. In TcMEc, residues R55 and T79, which correspond to R67 and R91 of HsME2 (Figure S1), are among the residues forming the binding pocket of **1** and R55 makes direct interactions with the inhibitor (Figure 2D). Eventually, mutations in the TcMEc allosteric pocket could prevent the binding of inhibitors and result in acquisition of drug resistance. However, if these mutations compromise the enzyme activation by aspartate, that can have negative effects on parasite viability and growth. These are relevant issues that need to be clarified by further investigation.

Superposition of the TcMEc structures of the ligand-free form and the complex with compound **1** shows that these two structures have the same conformation and domain arrangement (Figure S4). Presuming that the trypanosomal enzyme follows a similar allosteric activation model to that proposed for human ME2,[16] both TcMEc structures are in an open state. Therefore, compound **1** may lock the enzyme in an inactive open conformation, preventing aspartate binding and domains reorganization.

The allosteric inhibition pocket in TcMEc is formed by residues from domains A and B, from two distinct polypeptide chains (Figure 2D). The main interactions of **1** with the protein involve a π-stacking between the central phenyl ring of the inhibitor and residue F116, a hydrogen bond between the oxygen from the carboxamide with residue N23, and a network of hydrogen bonds between the sulfonamide group and residues Q52, R55, and N80. It is worth noting that residue T26, near Q52, is at a distance that would also allow for molecular interactions with the sulfonamide group of the inhibitor. Finally, the difluorophenyl and methoxyphenyl moieties appear to be engaged mainly in van der Waals interactions.

https://doi.org/10.1021/acsinfecdis.1c00231
ACS Infect. Dis. XXXX, XXX, XXX−XXX

Table 2. Target Inhibition, Binding, and Anti-*T. cruzi* activity of Compound 1 and Derivatives[c]

ID	R^1	X	R^2	R^3	IC_{50} (nM)	ΔTm (°C)[a]	EC_{50} (μM)[b]
1		H	H		29 ± 1	12.9	0.5 ± 0.3
30		H	H		8.0 ± 1.5	19.4	**n.d.**
31		H	H		9.4 ± 1.1	14.0	3.0 ± 1.6
32		H	H		13 ± 1	19.1	2.0 ± 1.2
33		H	H		28 ± 4	15.8	0.6 ± 0.2
34		H	H		44 ± 5	17.1	1.6 ± 0.8
35	H	Cl			**n.d.**	0.3	**n.a.**
36	H	Cl			**n.d.**	0.4	**n.a.**
37		Cl	H		6.5 ± 1.7	23.0	16 ± 10
38		Cl	H		17 ± 2	22.8	16 ± 7
39		Cl	H		22 ± 3	21.4	**n.d.**
40		Cl	H		76 ± 8	21.2	27 ± 3
41		H	H		34 ± 2	13.2	**n.d.**
42		H	H		29 ± 1	17.4	17 ± 3
43		H	H		**n.d.**	**n.a.**	**n.a.**

[a]Melting temperature (T_m) for TcMEc apo form is equal to 52.2 °C. [b]Benznidazole EC_{50} = 2,2 ± 0.4. [c]n.d.: not detected at highest assay concentration of 32 μM. n.a.: not assayed.

Synthesis of Compound 1 and Derivatives. Following the identification of TcMEc as a target for TCMDC-143108 (**1**), the synthesis of the original molecule and derivatives was projected. Despite **1** already being a potent inhibitor of TcMEc, new derivatives were planned to gain a deeper understanding on the determinants of binding, so as to allow for future modifications of the ligand to address potential druglike property issues.

The synthesis was devised in three steps consisting of (1) the formation of a diaryl sulfonamide (**6**−**17**) from the corresponding 3-nitrobenzenesulfonyl chlorides (**4** (X = H) and **5** (X = Cl)) and an aniline; (2) subsequent reduction of the nitro group and; (3) coupling of the resulting aniline (**18**−**29**) with a carboxylic acid or acyl chloride, which would yield the desired target compounds (Scheme 1). Compound **1** (TCMDC-143108) was prepared following this route to achieve the protein crystal complex. At first, we set out to explore different groups at the sulfonamide's aniline moiety, maintaining the 3,5-difluorobenzoic acid moiety. Overall, the synthesis of the target compounds proceeded smoothly, giving compound **1** and derivatives **30**−**35**. However, on reacting 3,5-difluorobenzoic acid chloride with chlorinated intermediates **24** (X = Cl, R_1 = 4-OMe) and **26** (X = Cl, R_1 = 2-F-4-OMe), an unexpected switch in reactivity favored acylation of the sulfonamide nitrogen, instead of the aniline nitrogen, as verified by NMR analyses. One could propose that a combination of aniline nucleophilicity reduction due to the neighboring chlorine atom and the electron-donating feature of the methoxy group *para* to the sulfonamide nitrogen accounted for the resulting products **35** and **36**. The four other chlorinated derivates (**25**, **27**−**29**), on the other hand, reacted as planned at the aniline nitrogen, yielding target compounds **37**−**40**. In order to also probe the binding pocket of the 3,5-difluorobenzamide moiety of compound **1**, three more compounds were prepared. First, a heterocyclic group was introduced under amino acid coupling conditions with aniline **19**, yielding pyrazine derivative **41**. Second, 3-fluoro-4-methoxybenzoic acid chloride was reacted with aniline **18** to afford compound **42**. Finally, we decided to prepare a compound lacking the amide functionality to assess its importance for ligand binding. Intermediate **19** was thus reacted with 4-methoxybenzaldehyde under reductive amination conditions to furnish benzylamine derivative **43**.

Effect of the Target Compounds on TcMEc Activity and Stability. The newly synthesized compounds were subjected to concentration-dependent enzymatic inhibition and differential scanning fluorimetry (nanoDSF) assays in order to calculate IC_{50} and melting temperatures (T_m) values over recombinant TcMEc (Table 2).

https://doi.org/10.1021/acsinfecdis.1c00231
ACS Infect. Dis. XXXX, XXX, XXX−XXX

The in house synthesized compound **1** and most of its derivatives returned IC_{50} values below 80 nM in the TcMEc inhibition assay. Compounds **30**−**33**, **37**, and **38**, with variations at the sulfonamide aniline moiety, but all bearing the 3,5-difluorobenzamide group, were usually better than reference hit **1** (IC_{50} = 29.0 nM), especially the ones with a 2-fluoro substitution pattern (**30**, **31**, and **37**), which displayed IC_{50} values below 10 nM. Only the trifluoromethoxylated analogues **34** and **40** proved to be less potent against TcMEc. Derivative **41**, bearing an electron-rich pyrazine moiety instead of the hydrophobic and electron-deficient 3,5-difluorobenzamide moiety still had an IC_{50} value similar to **1**, possibly enabled by the 2-fluorine atom on the sulfonamide aniline. Moving from a difluorobenzamide (**1**) to a 3-fluoro-4-methoxybenzamide (**42**) did not alter the IC_{50} value. Compounds **35** and **36** which were the products of sulfonamide acylation rather than aniline acylation in the final step, thus having a quite different structure, did not inhibit TcMEc activity and neither did benzylamine derivative **43**, indicating that the amide bond strongly contributes to binding interactions with the protein.

NanoDSF studies were also performed to evaluate the effect of the compounds on TcMEc thermal stability. In the absence of ligands, TcMEc returned a T_m of 52 °C. As observed in Table 2, compounds with IC_{50} values below 100 nM caused a marked stabilization of TcMEc, increasing its T_m by more than 12 °C. In line with the enzymatic inhibition data, compounds **35** and **36** had no effect over TcMEc thermal stability (ΔT_m < 1 °C). Interestingly, compounds **37**−**40**, which have a chlorine atom on the central phenyl ring, showed even higher ΔT_m values in comparison with their nonchlorinated pairs, **30** and **32**−**34**, respectively (Figure 3). The increase in ΔT_m among these four pairs of compounds varied from 3.6 to 5.4 °C. Altogether, these compounds indicate that chlorine atoms contribute with key interactions in stabilizing the TcMEc−inhibitor complexes, the nature of which could be revealed by crystallographic structures of TcMEc in complex with ligands **33**, **34**, **39**, and **40**.

Crystal Structures of TcMEc in Complex with New Sulfonamides and Structure−Activity Relationships. Crystal structures for six of the sulfonamide derivatives were obtained to support our proposals of structure−activity relationships (Table 1). Superposition of all complexes showed that all ligands occupy the same allosteric inhibition site with identical binding modes to that observed for compound **1** (Figure 4).

Looking first at complex TcMEc-**31** (Figure 5A), compound **31** (IC_{50} = 9.4 nM) bearing an additional fluorine atom at the 2-position of the aniline moiety in comparison to **1** (IC_{50} = 29.0 nM), the 3-fold increase in potency could be rationalized by the proximity of acidic protons of residues R55 and Q59 which seem to be engaging in hydrogen bonding with the electronegative fluorine atom (Figure 5B). These additional interactions are also featured in the TcMEc-**41** complex (Figure 5C); however, in this case, they seem to counteract a potential loss of potency due to the polar pyrazine ring at the other extremity of the ligand (IC_{50} (**41**) = 33.6 nM). In fact, nearby water molecules are found to connect the heterocyclic ring of ligand **41** to protein residues Y122 and R41 (Figure 5D), potentially imparting an entropy loss due to the solvation penalty. Next, a group of four protein−ligand complexes is worth discussing, namely, the ones with compounds **33**, **34** and **39**, **40**. Their aniline moieties are substituted with

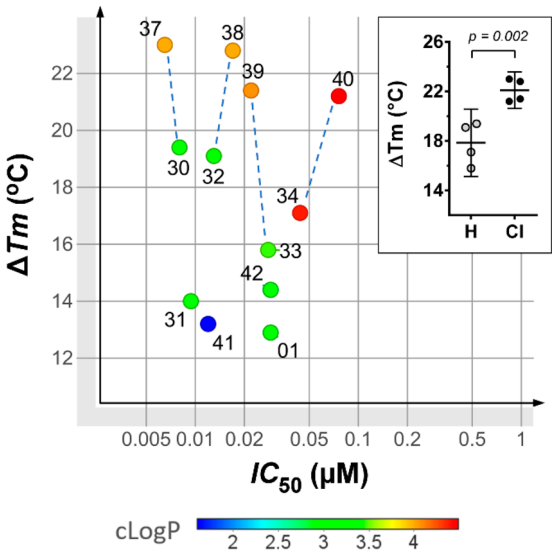

Figure 3. Inhibition and thermal stability of *T. cruzi* cytosolic malic enzyme by compound **1** and novel derivatives. IC_{50} values were calculated from concentration response inhibition assays. Melting temperatures (T_m) were calculated from nanoDSF denaturation curves. Dashed lines connect pairs of compounds that differ by the presence of a chlorine atom in the central phenyl ring. Symbols were colored according to *n*-octanol/water partition coefficient (cLogP) calculated using DataWarrior.[37] Inset plot shows ΔT_m values for **30** and **32**−**34** (gray circles, nonchlorinated molecules) and **37**−**40** (black circles, chlorinated compounds), with means and standard deviations represented for each group. *P* value calculated using paired *t* test in GraphPad Prism 6.00.

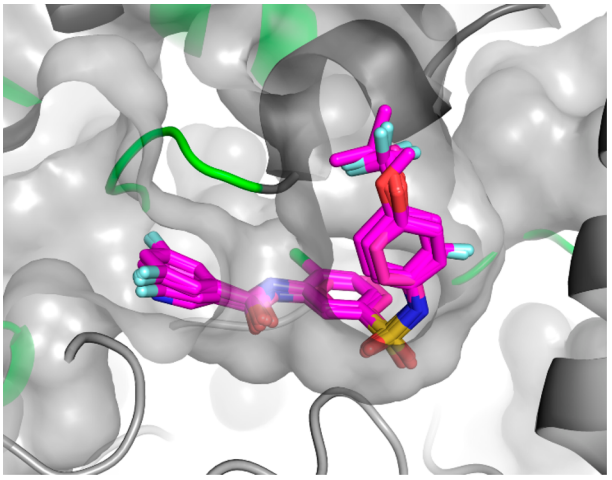

Figure 4. Superposition of the seven distinct sulfonamides for which a crystal structure was obtained in complex with TcMEc. All inhibitors (sticks with carbons in magenta) occupy the allosteric inhibition site located at the dimer interface through a similar binding mode. Molecules represented in the structure: **1**, **31**, **33**, **34**, and **39**−**41**. PDB IDs of complexes used to prepare the figure are reported in Table 1.

difluoromethoxyl and trifluoromethoxyl groups, respectively, and each pair was also prepared with an additional chlorine atom on the central phenyl ring. Although the position of compounds **33** and **34** in their respective binding site is identical (Figure 5E and F, respectively), and no major residue shifts were noted, a slight decrease in potency was noted moving from the difluoromethoxy to the trifluoromethoxy

https://doi.org/10.1021/acsinfecdis.1c00231
ACS Infect. Dis. XXXX, XXX, XXX−XXX

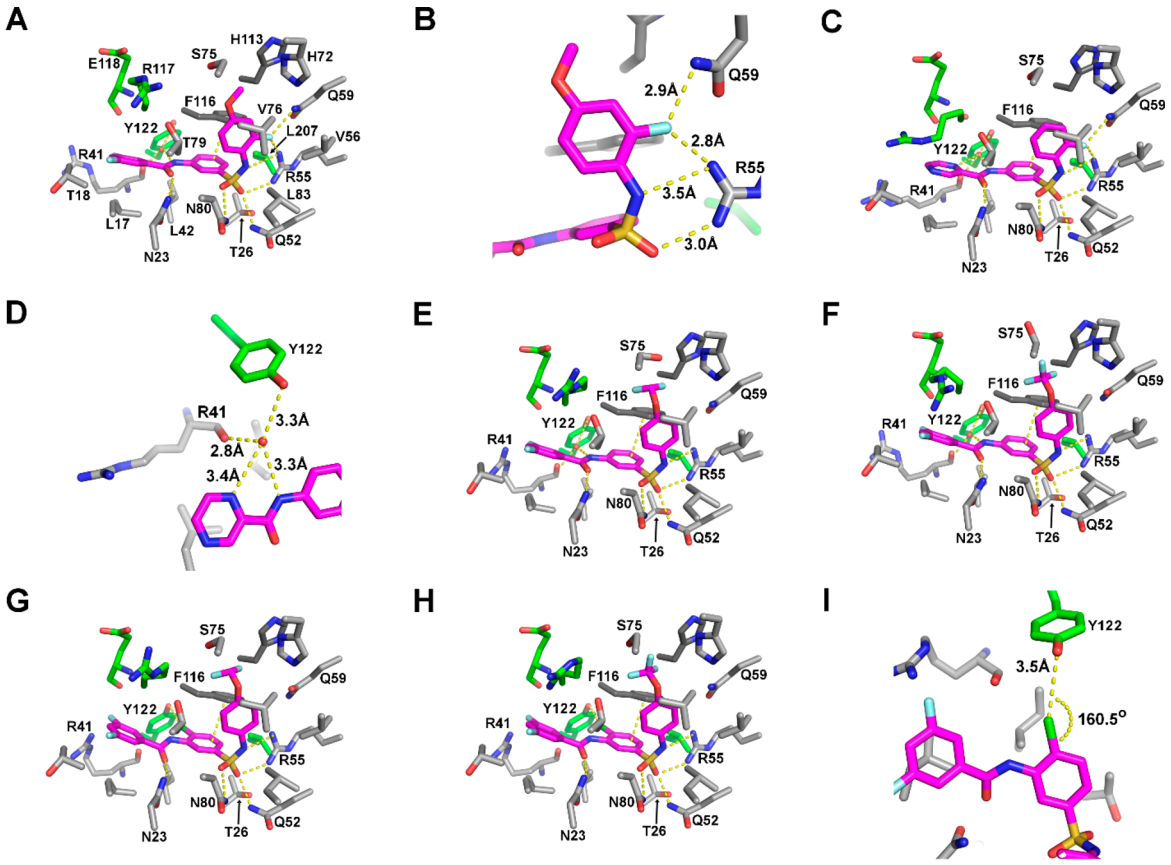

Figure 5. Binding mode of the TcMEc sulfonamide inhibitors revealed by crystal structures. Specific interactions of TcMEc residues with inhibitors are shown for compound **31** (A and B), **41** (C and D), **33** (E), **34** (F), **39** (G), and **40** (H and I). Amino acid residues have been colored according to the domain architecture (see Figure 2), and inhibitors are shown as sticks with magenta carbons.

substitution. Their chlorinated counterparts (**39** and **40** in Figure 5G and H, respectively), however, cause the expulsion of a water molecule near the Y122 residue in order to establish an interaction compatible with a halogen bond with Y122 (Figure 5I). In fact, the recorded geometric data (d[O···Cl] = 3.5 Å; angle O···Cl−C = 160.5°) are in line with this assumption.[38]

As mentioned earlier, while the addition of this chlorine atom did not necessarily increase the potency of these compounds in enzymatic assays, a clear contribution regarding protein stabilization was noted in nanoDSF assays (Table 2 and Figure 3). This makes sense, given that the halogen bond occurs between the ligand, which is mainly "tethered" by residues from one molecule of the dimer, and the Y122 residue from the other polypeptide chain forming the dimer. Finally, complexes of TcMEc with distinct derivatives (Figure 5) show that the carbonyl of the amide group of the inhibitors interacts with the protein residue N23, while the nitrogen interacts with a water molecule that forms an interaction network with residues Y122 and R41, helping to explain the loss of activity of compound **43** (Table 2) and reinforcing the relevance of this amide moiety for ligand binding.

In Vitro Activity of Sulfonamides against *T. cruzi* and Host Cells. The in vitro activity of TCMDC-143108 (**1**) was initially assessed by Peña and collaborators[18] in an image-based assay against intracellular *T. cruzi* (Y strain) amastigote forms infecting H9c2 rat cardiomyocytes. Here we used the same parasite strain, host cell line, and assay format to validate compound **1** and derivatives synthesized in house. Comparison of the EC_{50} value previously reported for TCMDC-143108 (see Figure 1C) and our synthetic version (**1**) (Table 2) shows that the results are in close agreement, allowing for the comparison of data from both reports. Among the new set of TcMEc inhibitors with IC_{50} < 100 nM, none of the derivatives were cytotoxic to host cells (rat cardiomyocytes) at 32 μM, the highest assayed concentration (HAC) in the phenotypic assays. Compounds **31**−**34** showed good dose−response profiles (Figure 6A), with calculated EC_{50} values equivalent to or better than that of benznidazole (BNZ), the reference drug in Chagas disease (Table 2). Compound **30**, however, bearing a 2-fluoroaniline moiety, was not active at 32 μM (HAC). The chlorinated compounds **37**, **38**, and **40** were effective against the parasite but worse than BNZ, with EC_{50}'s higher than 10 μM. Despite being good inhibitors of TcMEc, compounds **39** and **41** were not effective against the parasite at the HAC, while compound **42** was slightly less active than BNZ. Overall, derivatives **30** and **37**−**40** bearing an halogen at the aniline or central sulfone moiety, despite accounting for stronger protein binding or stabilization, showed a decreased or absence of in vitro efficacy. A similar trend was observed for compounds that had a more electron-rich amide moiety (**41** and **42**), in comparison to 3,5-difluorobenzamide. Thus, these observations suggest that electronic effects may modulate the anti-*T. cruzi* effectiveness of these sulfonamides. Whether it affects compound solubility, membrane permeability, or metabolic stability still needs to be investigated.

Looking further into the biological activity of the best compounds, image analyses of H9c2 cells infected by *T. cruzi*

https://doi.org/10.1021/acsinfecdis.1c00231
ACS Infect. Dis. XXXX, XXX, XXX−XXX

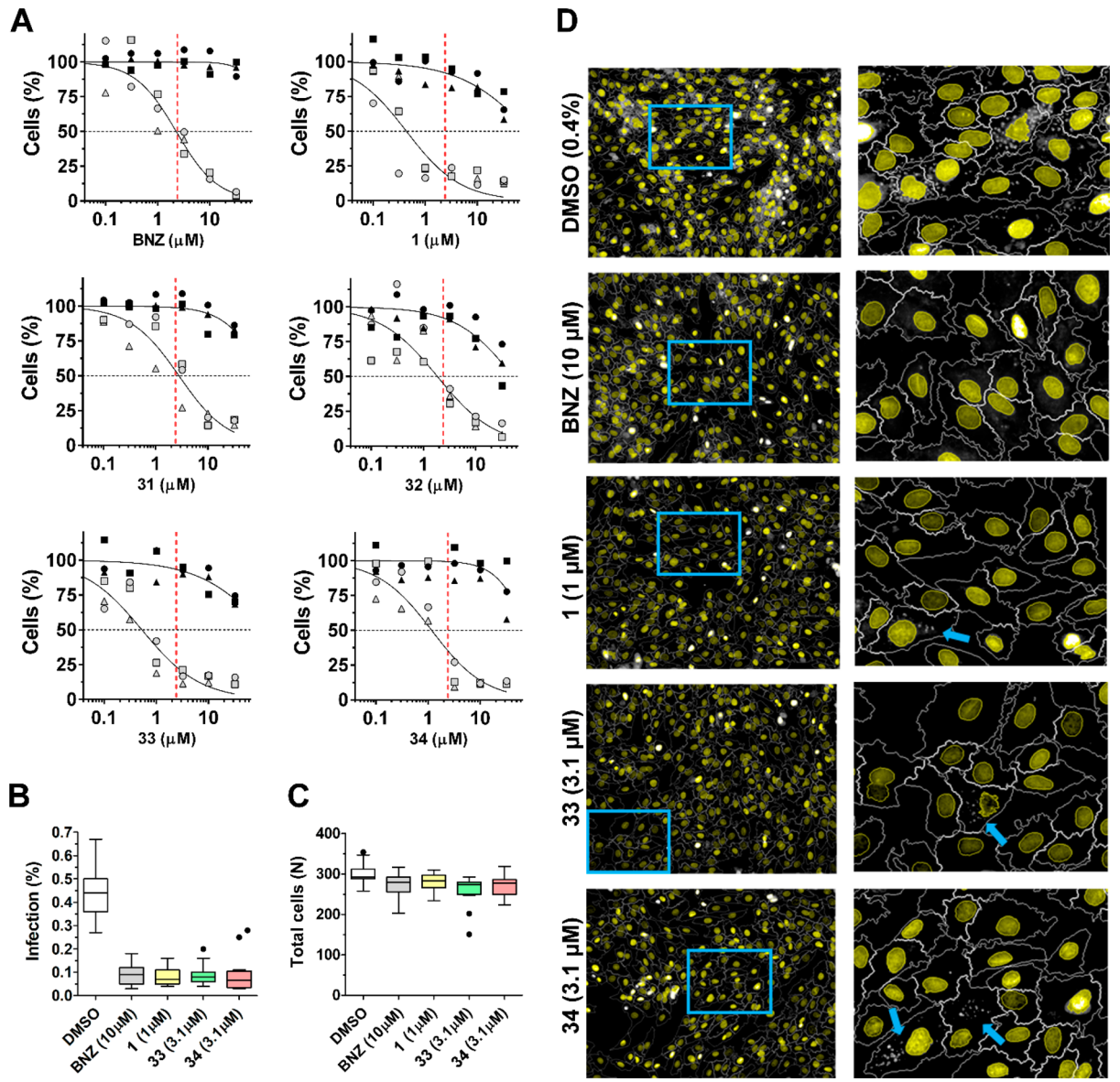

Figure 6. Concentration−response curves and image analyses of *T. cruzi* (Y strain) intracellular assays. (A) Normalized concentration−response curves for quantification of host cells (black circles) and intracellular *T. cruzi* (white circles). Dashed red line indicates the correspondent EC_{50} for benznidazole (BNZ). Box plots for percentage of infected cells (B) and total host cells (C) per image (N = 15). (D) Representative images (left) and zoom from blue boxes (right) for DMSO, BNZ, and compounds **1**, **33**, and **34**. Host cell nuclei are colored in yellow, and *T. cruzi* amastigotes appear as white spots in the cytoplasm of infected cells (indicated by blue arrows).

(Y strain) and treated for 72 h with 1 μM **1** and 3.1 μM **33** and **34** showed a significant reduction in the percentage of infected cells, a similar phenotype requiring 10 μM BNZ (Figure 6B). Moreover, at those concentrations, compounds had no significant impact over the count of total cells, which further supports the absence of cytotoxicity in rat cardiomyocytes (Figure 6C). Nevertheless, a detailed inspection of the images permits one to view cells with putative remaining parasites (Figure 6D). Whether these are dormant *T. cruzi* amastigotes[39] that could lead to the recovery of infection after removing drug pressure remains to be investigated.

CONCLUSIONS

According to the World Health Organization, 6−7 millon people worldwide are infected with *T. cruzi*. The current chemotherapy relies on only two drugs, benznidazole or nifurtimox, with toxicity issues and low efficacy for the chronic stage of the disease. Therefore, new anti-Chagas drug discovery initiatives should prioritize molecules that are effective against the intracellular forms of the parasite which are associated with chronic Chagas disease. Recently, high-throughput phenotypic screenings revealed a significant number of compounds active against intracellular *T. cruzi* forms. Characterization of the mode of action and target identification for phenotypic hits can accelerate their development into new drug candidates. In the present work, we demonstrate that the *T. cruzi* cytosolic malic enzyme (TcMEc) is the target for three different compounds from the Chagas Box. One of these new TcMEc inhibitors, TCMDC-143108 (**1**), and 14 new analogues where synthesized and tested for target inhibition, efficacy against *T. cruzi* amastigotes, and host cell cytotoxicity. Overall, four compounds of this series showed nanomolar target inhibition, low

https://doi.org/10.1021/acsinfecdis.1c00231
ACS Infect. Dis. XXXX, XXX, XXX−XXX

micromolar efficacy against the intracellular parasite, and no cytotoxicity for the host cells. Moreover, the TcMEc crystal structure and complexes with seven new inhibitors were described here for the first time.

The target−inhibitor complexes reveal that these sulfonamides bind to the aspartate allosteric activation site, located at the enzyme's dimeric interface, blocking it in an inactive state. The new inhibitors all bind in a very similar fashion, allowing the identification of the most relevant interactions and the establishment of clear structure−activity relationships. It is worth noting that sulfonamides are present in several FDA-approved drugs and are readily accessible from a synthetic point of view, thus making the new TcMEc inhibitors a promising starting point for further drug development in Chagas disease. Moreover, the here reported TcMEc inhibitors could now be used in chemical biology studies to investigate target engagement and TcMEc essentiality for distinct *T. cruzi* forms.

MATERIALS AND METHODS

Reagents. Chagas Box samples were provided by GSK (Tres Cantos, Spain). TcMEc and TcMEm were expressed and purified as previously described.[5,17]. Resazurin, $NADP^+$, malate, aspartate, $MnCl_2$, tris(hydroxymethyl)aminomethane, NaCl, paraformaldehyde (PFA), DMSO, and Dulbecco's modified Eagle's medium (DMEM) were supplied by Merck-Sigma-Aldrich. *Clostridium kluyveri* diaphorase was bought from Worthington Biochemical. Triton X-100 was obtained from Serva. Fetal bovine serum (FBS) was bought from Vitrocell. Penicillin streptomycin solution (10,000 U/mL and 10 ,000 μg/mL, respectively) and Hoechst 33342 were ordered from ThermoFisher. Microplates were obtained from Greiner Bio-One.

Cloning. The DNA fragment encoding for the TcMEc residues ranging from Q12 to L565 (TcΔMEc) was amplified from pET28_TcMEc[5] using the primers 5′-GCGGATCCC-ATATGCAAGGAAGAGCAATCCTGACG-3′ and 5′-GCT-AGTTATTGCTCAGCGGTG-3′and subcloned into the *Bam*HI and *Eco*RI restriction sites of pET-SUMO.

Protein Production, Purification, and Crystallization. Production and purification of TcMEc and TcΔMEc followed the protocols described previously,[5,17] with the exception that for TcΔMEc the His-SUMO tag was cleaved with ULP-1 protease for 16 h at 4 °C before the size exclusion chromatography. Crystals of TcΔMEc were grown by the vapor diffusion method at 18 °C by mixing 3 μL of protein (5 mg/mL, in 10 mM TRIS-HCl pH 8.0, 30 mM NaCl, 2 mM $MnCl_2$, 10 mM aspartate) with 3 μL reservoir solution (100 mM HEPES pH 7.0, 1.4 M trisodium citrate). For complexes, 24 h previous to data collection, TcΔMEc crystals were transferred to drops containing 1.8 μL of reservoir solution and 0.2 μL of inhibitors stock solution (10 mM in 100% DMSO).

Screening of Chagas Box against TcMEc and TcMEm. A total of 218 compounds from the Chagas Box were provided by GSK preplated in 384-well microplates at 1 mM in 100% DMSO. Plates contained either 100 or 200 nL of compounds per well. These plates were used to screen the compounds in duplicates, at concentrations of 5 and 10 μM, against TcMEc and TcMEm. ME reactions were coupled to diaphorase, that uses NADPH to produce the fluorescent molecule resorufin from resazurin.[17,40,41] Each well of the plates was filled using a Multidrop Combi reagent dispenser (Thermo-Fisher) to a final volume of 20 μL. For TcMEc, the reactions were performed in the following conditions: 20 μM $NADP^+$, 2 mM $MnCl_2$, 10 μM resazurin, 0.4 mM aspartate, 2 U/mL diaphorase, 0.3 nM TcMEc, and 1.3 mM malate. Similarly, for TcMEm, the assays were set as follows: 10 μM $NADP^+$, 2 mM $MnCl_2$, 10 μM resazurin, 2 U/mL diaphorase, 0.8 nM TcMEm, and 1.0 mM malate. The reactions for both enzymes were performed in an assay buffer containing 50 mM Tris-HCl, 50 mM NaCl, and 0.01% triton X-100, pH 7.5. Reactions were always started by the addition of malate and followed by measuring the formation of resorufin (λ_{Exc} 545 ± 20 nm; λ_{Em} 600 ± 40 nm) with a plate reader (CLARIOstar, BMG LabTech). Velocities (RFU/min) of positive (100% activity; DMSO) and negative (0% activity, no enzyme) controls were used for sample data normalization.

Dose−Response Enzyme Inhibition Assays. IC_{50} values for compounds were determined using the ME−diaphorase−resorufin coupled assay by measuring the reaction velocities at varying inhibitors concentrations. Serial dilutions of compounds were prepared in microplates using Versette (Thermo-Fisher) with DMSO as the solvent. Reactions were prepared in quadruplicate in 384-well plates by transferring 45 μL of a reagent mix (0.48 nM TcMEc or 1.78 nM TcMEm; 22.2 μM NADP+, 1.11 U/mL diaphorase; 444 μM aspartate; 2.22 mM $MnCl_2$, and 11.1 μM resazurin in reaction buffer containing 50 mM Tris-HCl, 50 mM NaCl, and 0.01% triton X-100, pH 7.5) with Multidrop combi (ThermoFisher); 1 μL of the compound solutions with Versette; and 4 μL of malate 16.25 mM for TcMEc and 12.5 mM for TcMEm with Versette. Positive controls (100% activity) were prepared with all reaction components except compounds (DMSO only). The enzymatic activity was followed measuring the formation of resorufin with a CLARIOstar plate reader (BMG LabTech) in the fluorescent mode (λ_{Exc} 545 ± 20 nm; λ_{Em} 600 ± 40 nm). The velocities obtained were normalized by the controls, and the IC_{50} values were calculated by nonlinear regression of the data using GraphPad Prism software.

Nanoscale Differential Scanning Fluorimetry (nanoDSF) Assays. A Prometheus NT.48 nanoDSF instrument (nanoTemper Technologies, Munich, Germany) was employed in the study of thermal stabilization effects of TcΔMEc inhibitors. Samples were prepared by diluting purified TcΔMEc to 10 μM in a buffer containing Tris 10 mM (pH 8.0), NaCl 30 mM, and inhibitors at 20 μM. Because the small molecules were diluted in DMSO, a final concentration of 1.25% of the solvent was obtained. Capillaries filled with samples were placed on the sample holder, and a temperature gradient from 15 to 95 °C (1 °C/min steps) was applied. Intrinsic protein fluorescence was recorded at 330 and 350 nm. The fluorescence of the small molecules was checked before measurements. Melting temperatures (T_m) were obtained by analysis of the melting curves using the software PR.Stability Analysis, supplied by the instrument manufacturer.

X-ray Diffraction and Structure Determination. Data for ligand free TcΔMEc was collected on beamline I03 at the Diamond Light Source (UK), while sets for TcΔMEc in complex with sulfonamide inhibitors were collected at the Brazilian Synchrotron Light Laboratory (LNLS) beamline W01B-MX2. All data sets were acquired at 100° K and integrated using XDS.[42] Using CCP4 suite,[43] data were scaled with AIMLESS[44] and TcMEc structures were determined by molecular replacement with PHASER[45] using a combination of different domains as search models, as follows: domain-A, residues 11−128 (PDB 1GZ3),[26] domain-B, residues 129−274

https://doi.org/10.1021/acsinfecdis.1c00231
ACS Infect. Dis. XXXX, XXX, XXX−XXX

(PDB 3WJA),[11] domain-C, residues 275−467 (PDB 3WJA), and domain-D, residues 468−539 (PDB 1GQ2).[12] Structures were refined with Phenix,[46] REFMAC,[47] and COOT.[48] pdb_extract[49] was used to prepare files for deposition in the Protein Data Bank (PDB). Crystallographic statistics and PDB codes of deposited structures are reported in Table 1. Molecular figures were prepared in PYMOL v.1.8 (Schrodinger, LLC, New York, NY, USA).

T. cruzi Intracelullar Amastigote Image-Based Assays. Methodology for cell-based assays of intracellular *T. cruzi* have been described elsewhere.[50] Briefly, LLC-MK2 (green monkey kidney epithelial cells) and H9c2 (rat cardiomyocytes) were cultivated in DMEM supplemented with 10% heat-inactivated fetal bovine serum (FBS) and antibiotics (100 U/mL penicillin; 100 μg/mL streptomycin). LLC-MK2 infected with *T. cruzi* (Y strain) was maintained in DMEM medium supplemented with 2% FBS and antibiotics. Trypomastigotes were collected from supernatant after 4−5 days of infection. Cells were always incubated in T-flasks at 37 °C, 5% CO_2, and >95% humidity.

Compounds to be used in cellular image-based assays were dissolved and/or serial diluted in DMSO. Serial dilutions were performed applying a half-log factor. Intermediary plates were prepared diluting compounds in fresh DMEM medium using a proportion of 1:99.

T. cruzi trypomastigotes (5×10^5 cells) collected from infected LLC-MK2 cells were used to infect H9c2 rat cardiomyocytes (1×10^6 cells) overnight (16−18 h), in 75 cm^2 T-flasks. Then, cells were washed with phosphate buffered solution (PBS) to remove extracellular parasites, trypsinized, and resuspended in fresh DMEM medium to a concentration of 2.2×10^4 cells/mL. A volume of 45 μL of this cellular suspension was dispensed into 384-well assay plates (1×10^3 cells per well) using a Multidrop Combi system (Thermo Fisher Science). Plates were incubated for addition 48 h for *T. cruzi* differentiation into intracellular amastigotes. Subsequently, 30 μL of samples from intermediary plates was transferred to assay plates in such a way that the DMSO concentration was reduced to 0.4%. After 72 h of incubation (treatment period), cells were fixed with 4% paraformaldehyde (PFA) and stained with Hoechst 33342 (4 μg/mL in PBS). Five images per well were acquired with the fluorescence microscope Operetta (PerkinElmer, Hamburg, DE) using a 20× long WD objective and processed in Columbus software (PerkinElmer, Hamburg, DE) to identify host cell nuclei, cytoplasm area, and spots in the cytoplasm. Infected cells were defined as cells with at least three spots in the cytoplasm area. The Infection ratio corresponds to infected cells/total cells per well. Total cells, infected cells, and infection ratio data were analyzed and plotted with GraphPad Prism software.

Synthetic Chemistry. Reagents and anhydrous solvents were purchased from Sigma-Aldrich Brasil Ltd.a for carrying out the reactions and from Labsynth Produtos para Laboratórios Ltd.a (analytical grade) for workup, and were used without further purification unless specified otherwise. Anhydrous pyridine was distilled from and stored over potassium hydroxide. Reactions were monitored by thin-layer chromatography (TLC) on silica gel 60 F254 aluminum sheets and exposed to UV radiation, followed by treatment with adequate stains and heating. Chromatographic separations were carried out on Merck 60 silica gel (230−400 mesh). Melting points (mp) were recorded on a PF 1500 FARMA apparatus with a heating rate of 5 °C/min and were uncorrected. ^{1}H NMR and ^{13}C NMR data were recorded on a Varian 500 MHz or Varian 600 MHz spectrometer using TMS as the internal standard, or the residual nondeuterated solvent. Chemical shifts (δ) were expressed in ppm, and multiplicities were reported as singlet (s), broad signal (bs), doublet (d), double doublet (dd), triplet (t), apparent triplet (at), double triplet (dt), quartet (q), double apparent quartet (daq), apparent quartet (aq), quintuplet (quint), heptuplet (hept), multiplet (m), and triple triplet (tt). Coupling constants (J) are expressed in Hertz (Hz) and refer to $^2J_{HH}$ or $^3J_{HH}$, unless specified otherwise. High-resolution electrospray ionization mass spectrometry (HRMS-ESI) and target compound purity assessments were performed on a Waters Acquity H-Class UPLC system coupled to a PDA detector and a Bruker Impact II mass spectrometer.

*Method A. General Procedure for the Synthesis of Sulfonamides (**6**−**17**).* To a solution of nitrobenzenesulfonyl chloride (1.13 mmol; 1.0 equiv) and aniline (1.35 mmol; 1.2 equiv) in anhydrous dichloromethane (3.8 mL; 0.3M) was added anhydrous pyridine (2.26 mmol; 2.0 equiv) dropwise at room temperature over an argon atmosphere. TLC analysis showed complete consumption of the starting sulfonyl chloride after 3 h. The reaction mixture was diluted with chloroform (7 mL), washed with a 1 M HCl solution (10 mL) and brine (10 mL), dried over $MgSO_4$, and filtered, and the solvent was removed in vacuo. When necessary, the dark red oil was taken up in methanol (10 mL) and passed through a pad of activated charcoal, yielding a clear to light yellow solution, which after drying in vacuo furnished the desired sulfonamide without further purification.

*Method B. General Procedure for the Synthesis of Amines (**18**−**29**).* A suspension of the nitro derivative (0.71 mmol; 1.0 equiv) and tin(II) chloride dihydrate (3.57 mmol; 5.0 equiv) in ethyl acetate (7.1 mL; 0.1M) was heated at reflux for 2 h. After cooling, the reaction mixture was diluted with water (5 mL), and the pH was adjusted to 7−8 by the addition of a saturated aqueous $NaHCO_3$ solution (approximately 40 mL). The product was extracted into ethyl acetate (2 × 50 mL), washed with water (2 × 50 mL) and brine (50 mL), dried over $MgSO_4$, and filtered, and the solvent was removed in vacuo to deliver the desired amine, which was used without further purification, unless stated otherwise. N.B.: The aqueous layers containing tin residues were discarded in a separate container and disposed of as hazardous waste.

*Method C. General Procedure for the Synthesis of Target Compounds (**1**, **30**−**40**).* To a solution of the amine derivative (0.18 mmol; 1.0 equiv) and 3,5-difluorobenzoyl chloride (0.27 mmol; 1.5 equiv) in an anhydrous solvent (DMF, MeCN, or CH_2Cl_2) (0.9 mL; 0.2M) was added *N*-methylmorpholine (0.54 mmol; 3.0 equiv) at room temperature under an argon atmosphere. Usually, the reaction was completed after 1−2 h, upon which time the mixture was diluted with ethyl acetate (4 mL), washed with 1 M HCl (2−5 mL) and brine (2 × 2−5 mL), dried over $MgSO_4$, and filtered, and the solvent was removed in vacuo. Purification of the desired product was achieved either through crystallization or by column chromatography, as described for each compound.

*N-(4-Methoxyphenyl)-3-nitrobenzenesulfonamide (**6**).* Method A. Yield: 68%; off white solid; mp 132−133 °C (135 °C[51]); δ_H (500 MHz; $CDCl_3$) 8.58 (1 H, t, J 1.9), 8.40 (1 H, daq, J 8.2, 1.0), 7.98 (1 H, dt, J 8.7, 1.2), 7.65 (1 H, t, J 8.0), 7.00 (2 H, d, J 8.9), 6.79 (2 H, d, J 9.0), 3.77 (3 H, s); δ_C (125.5 MHz; $CDCl_3$) 158.6, 148.2, 141.1, 132.9, 130.3, 127.7,

https://doi.org/10.1021/acsinfecdis.1c00231
ACS Infect. Dis. XXXX, XXX, XXX−XXX

127.3, 126.0, 122.5, 114.8, 55.5; HRMS-ESI calcd for $C_{13}H_{16}N_3O_5S^+$ $[M + NH_4]^+$: 326.0805, found: 326.0811.

*N-(2-Fluorophenyl)-3-nitrobenzenesulfonamide (**7**).* Method A. Yield: 76%; off white solid, mp 121 °C; δ_H (500 MHz; $CDCl_3$) 8.61 (1 H, t, *J* 2.0), 8.41 (1 H, daq, *J* 8.2, 0.9), 8.07 (1 H, daq, *J* 7.9, 0.9), 7.67 (1 H, t, *J* 8.0), 7.64−7.60 (1 H, m), 7.19−7.13 (1 H, m), 6.99−6.95 (1 H, m), 6.86 (1 H, bs); δ_C (125.5 MHz; $CDCl_3$) 154.4 (d, $^1J_{CF}$ 245.5), 148.2, 140.1, 132.6, 130.5, 127.7, 127.57 (d, $^3J_{CF}$ 7.6), 125.15 (d, $^4J_{CF}$ 3.9), 124.6, 123.35 (d, $^2J_{CF}$ 12.4), 122.5, 115.72 (d, $^2J_{CF}$ 19.4); HRMS-ESI calcd for $C_{12}H_9FN_2NaO_4S^+$ $[M + Na]^+$: 319.0159, found: 319.0148.

*N-(2-Fluoro-4-methoxyphenyl)-3-nitrobenzenesulfonamide (**8**).* Method A. Yield: 98%; dark brown solid; mp 104 °C; δ_H (500 MHz; $CDCl_3$) 8.57 (1 H, t, *J* 1.9), 8.41 (1 H, daq, *J* 8.8, 1.0), 8.01 (1 H, d, *J* 7.8), 7.66 (1 H, t, *J* 8.1), 7.48 (1 H, t, *J* 9.0), 6.72 (1 H, daq, *J* 8.9, 1.3), 6.58 (1 H, bs), 6.49 (1 H, dd, *J* 11.9, 2.8), 3.76 (3 H, s); δ_C (125.5 MHz; $CDCl_3$) 159.7 (d, $^3J_{CF}$ 10.4), 156.5 (d, $^1J_{CF}$ 246.4), 148.1, 141.0, 132.7, 130.3, 128.2 (d, $^2J_{CF}$ 1.7), 127.5, 122.5, 115.2 (d, $^3J_{CF}$ 13.3), 110.5 (d, $^4J_{CF}$ 3.1), 102.0 (d, $^2J_{CF}$ 23.2), 55.7; HRMS-ESI calcd for $C_{13}H_{11}FN_2NaO_5S^+$ $[M + Na]^+$: 349.0265, found: 349.0281.

*N-(Benzo[d][1,3]dioxol-5-yl)-3-nitrobenzenesulfonamide (**9**).* Method A. Yield: 81%; off white solid; mp 143−144 °C; δ_H (500 MHz; DMSO-d_6) 10.26 (1 H, s), 8.46−8.44 (1 H, m), 8.06 (1 H, daq, *J* 7.9, 0.9), 7.86−7.83 (1 H, m), 6.77 (1 H, d, *J* 8.3), 6.66 (1 H, d, *J* 2.1), 6.48 (1 H, dd, *J* 8.3, 2.1), 5.96 (2 H, s); δ_C (125.5 MHz; DMSO-d_6) 147.9, 147.6, 145.0, 140.7, 132.7, 131.3, 130.4, 127.5, 121.5, 115.7, 108.4, 104.2, 101.5; HRMS-ESI calcd for $C_{13}H_{10}N_2NaO_6S^+$ $[M + Na]^+$: 345.0152, found: 345.0153.

*N-(4-(Difluoromethoxy)phenyl)-3-nitrobenzenesulfonamide (**10**).* Method A. Yield: 81%; white fluffy solid; mp 106−107 °C; δ_H (500 MHz; DMSO-d_6) 10.59 (1 H, s), 8.48 (1 H, t, *J* 1.8), 8.46 (1 H, daq, *J* 8.2, 1.1), 8.11 (1 H, daq, *J* 7.9, 0.9), 7.86 (1 H, t, *J* 8.1), 7.12 (1 H, t, $^2J_{HF}$ 74.1), 7.13 (2 H, d, *J* 9.2), 7.08 (2 H, d, *J* 9.0); δ_C (125.5 MHz; DMSO-d_6) 147.96 (t, $^3J_{CF}$ 3.2), 147.91, 140.8, 133.8, 132.6, 131.4, 127.7, 123.0, 121.4, 119.9, 116.2 (t, $^1J_{CF}$ 257.9); HRMS-ESI calcd for $C_{13}H_{10}F_2N_2NaO_5S^+$ $[M + Na]^+$: 367.0171, found: 367.0169.

*N-(4-(Trifluoromethoxy)phenyl)-3-nitrobenzenesulfonamide (**11**).* Method A. Yield: 80%; white fluffy solid; mp 134−135 °C; δ_H (500 MHz; DMSO-d_6) 10.59 (1 H, s), 8.49−8.45 (2 H, m), 8.14 (1 H, daq, *J* 7.9, 0.8), 7.87 (1 H, t, *J* 8.0), 7.28 (2 H, d, *J* 8.4), 7.20 (2 H, d, *J* 9.1); δ_C (150 MHz; DMSO-d_6) 148.0, 145.07 (q, $^3J_{CF}$ 1.8), 140.7, 136.1, 132.6, 131.5, 127.8, 122.4, 122.3, 121.4, 120.0 (q, $^1J_{CF}$ 256.1); HRMS-ESI calcd for $C_{13}H_9F_3N_2NaO_5S^+$ $[M + Na]^+$: 385.0076, found: 385.0085.

*4-Chloro-N-(4-methoxyphenyl)-3-nitrobenzenesulfonamide (**12**).* Method A. Yield: 65%; off white solid; mp 78−79 °C; δ_H (500 MHz; $CDCl_3$) 8.20 (1 H, d, *J* 2.1), 7.76 (1 H, dd, *J* 8.5, 2.2), 7.62 (1 H, d, *J* 8.4), 7.01 (2 H, d, *J* 9.0), 6.81 (2 H, d, *J* 9.0), 3.78 (3 H, s); δ_C (125.5 MHz; $CDCl_3$) 158.8, 147.7, 139.1, 132.8, 131.9, 131.3, 127.3, 126.2, 124.6, 114.9, 55.5; HRMS-ESI calcd for $C_{13}H_{15}ClN_3O_5S^+$ $[M + NH_4]^+$: 360.0415, found: 360.0429.

*4-Chloro-N-(2-fluorophenyl)-3-nitrobenzenesulfonamide (**13**).* Method A. Yield: 87%; light orange solid; mp 132−133 °C; δ_H (500 MHz; DMSO-d_6) 10.57 (1 H, s), 8.38 (1 H, d, *J* 2.1), 8.01 (1 H, d, *J* 8.4), 7.97 (1 H, dd, *J* 8.5, 2.1), 7.30−7.16 (4 H, m); δ_C (125.5 MHz; DMSO-d_6) 156.2 (d, $^1J_{CF}$ 247.9), 147.3, 140.1, 133.2, 131.3, 129.9, 128.5 (d, $^3J_{CF}$ 7.7), 127.7, 125.0 (d, $^4J_{CF}$ 3.7), 124.0, 123.3 (d, $^3J_{CF}$ 12.9), 116.3 (d, $^2J_{CF}$ 19.7); H

RMS-ESI calcd for $C_{12}H_8ClFN_2NaO_4S^+$ $[M + Na]^+$: 352.9770, found: 352.9762.

*4-Chloro-N-(2-fluoro-4-methoxyphenyl)-3-nitrobenzenesulfonamide (**14**).* Method A. Yield: 67%; off white solid; mp 118−119 °C; δ_H (500 MHz; $CDCl_3$) 8.18 (1 H, d, *J* 2.1), 7.81 (1 H, dd, *J* 8.4, 2.2), 7.64 (1 H, d, *J* 8.4), 7.45 (1 H, t, *J* 9.0), 6.72 (1 H, daq, *J* 8.9, 1.3), 6.58 (1 H, bs), 6.54 (1 H, dd, *J* 11.7, 2.7), 3.78 (3 H, s); δ_C (125.5 MHz; $CDCl_3$) 159.94 (d, $^3J_{CF}$ 10.5), 156.6 (d, $^1J_{CF}$ 246.6), 147.6, 139.1, 132.8, 132.0, 131.1, 128.39 (d, $^2J_{CF}$ 1.7), 124.6, 114.84 (d, $^3J_{CF}$ 13.4), 110.61 (d, $^4J_{CF}$ 3.2), 102.05 (d, $^2J_{CF}$ 23.2), 55.8; HRMS-ESI calcd for $C_{13}H_{10}ClFKN_2O_5S^+$ $[M + K]^+$: 398.9615, found: 398.9620.

*N-(Benzo[d][1,3]dioxol-5-yl)-4-chloro-3-nitrobenzenesulfonamide (**15**).* Method A. Yield: 88%; brown solid; mp 129−130 °C; δ_H (500 MHz; $CDCl_3$) 8.22 (1 H, d, *J* 2.0), 7.81 (1 H, dd, *J* 8.5, 2.0), 7.65 (1 H, d, *J* 8.5), 6.80 (1 H, bs), 6.69 (1 H, s), 6.69−6.67 (2 H, m), 6.46 (1 H, dd, *J* 8.2, 1.0), 5.98 (2 H, s); δ_C (125.5 MHz; $CDCl_3$) 148.5, 147.7, 146.9, 139.0, 132.2, 132.0, 131.3, 128.5, 124.6, 117.8, 108.5, 106.1, 101.9; HRMS-ESI calcd for $C_{13}H_{13}ClN_3O_6S^+$ $[M + NH_4]^+$: 347.0208, found: 374.0199.

*4-Chloro-N-(4-(difluoromethoxy)phenyl)-3-nitrobenzenesulfonamide (**16**).* Method A. Yield: 99%; orange oil; δ_H (500 MHz; $CDCl_3$) 8.26 (1 H, d, *J* 2.1), 7.82 (1 H, dd, *J* 8.5, 1.8), 7.66 (1 H, d, *J* 8.5), 7.12 (2 H, d, *J* 4.7), 7.08 (2 H, d, *J* 4.7), 6.94 (1 H, bs), 6.48 (1 H, t, $^2J_{HF}$ 73.3); δ_C (125.5 MHz; $CDCl_3$) 149.4 (t, $^3J_{CF}$ 3.0), 147.8, 140.8, 138.9, 133.1, 132.3, 132.2, 131.2, 124.6, 124.5, 121.0, 115.5 (t, $^1J_{CF}$ 261.4); HRMS-ESI calcd for $C_{13}H_{13}ClF_2N_3O_5S^+$ $[M + NH_4]^+$: 396.0227, found: 396.0215.

*4-Chloro-N-(4-(trifluoromethoxy)phenyl)-3-nitrobenzenesulfonamide (**17**).* Method A. Yield: 96%; yellow oil; δ_H (500 MHz; $CDCl_3$) 8.29 (1 H, d, *J* 2.1), 7.83 (1 H, dd, *J* 8.3, 2.2), 7.67 (1 H, d, *J* 8.4), 7.18−7.14 (4 H, m), 7.02 (1 H, bs); δ_C (125.5 MHz; $CDCl_3$) 147.9, 147.4 (q, $^3J_{CF}$ 1.9), 138.9, 133.7, 133.1, 132.5, 131.1, 124.6, 123.9, 122.4, 120.3 (q, $^1J_{CF}$ 257.9); HRMS-ESI calcd for $C_{13}H_9ClF_3N_2O_5S^+$ $[M + H]^+$: 396.9867, found: 396.9855.

*3-Amino-N-(4-methoxyphenyl)benzenesulfonamide (**18**).* Method B. Yield: 94%; off white solid; mp 179−181 °C (180−181 °C[52]); δ_H (600 MHz; DMSO-d_6) 9.74 (1 H, s), 7.11 (1 H, t, *J* 7.9), 6.98 (2 H, d, *J* 8.9), 6.89 (1 H, t, *J* 2.0), 6.81−6.78 (3 H, m+d, *J* 9.0), 6.69 (1 H, dd, *J* 8.0, 2.2), 5.53 (2 H, s), 3.67 (3 H, s); δ_C (150 MHz; DMSO-d_6) 156.3, 149.2, 140.1, 130.5, 129.4, 123.0, 117.3, 114.2, 113.3, 111.3, 55.1; HRMS-ESI calcd for $C_{13}H_{15}N_2O_3S^+$ $[M + H]^+$: 279.0798, found: 279.0801.

*3-Amino-N-(2-fluorophenyl)benzenesulfonamide (**19**).* Method B. Yield: 92%; off white solid; mp 161−162 °C; δ_H (500 MHz; DMSO-d_6) 9.95 (1 H, bs), 7.22 (1 H, t, *J* 8.5), 7.17−7.12 (3 H, m), 7.11−7.08 (1 H, m), 6.93 (1 H, t, *J* 2.0), 6.82 (1 H, daq, *J* 7.7, 0.9), 6.73 (1 H, daq, *J* 8.1, 1.1), 5.55 (2 H, bs); δ_C (125.5 MHz; DMSO-d_6) 155.4 (d, $^1J_{CF}$ 247.2), 149.3, 140.6, 129.5, 126.82 (d, $^2J_{CF}$ 7.5), 125.8, 124.79 (d, $^3J_{CF}$ 12.8), 124.5 (d, $^4J_{CF}$ 3.8), 117.6, 115.93 (d, $^2J_{CF}$ 19.6), 113.2, 111.0; HRMS-ESI calcd for $C_{12}H_{12}FN_2O_2S^+$ $[M + H]^+$: 267.0598, found: 267.0599.

*3-Amino-N-(2-fluoro-4-methoxyphenyl)-benzenesulfonamide (**20**).* Method B. Yield: 96%; light violet solid; mp 149−150 °C; δ_H (500 MHz; $CDCl_3$) 9.58 (1 H, bs), 7.13 (1 H, t, *J* 7.9), 7.02 (1 H, t, *J* 9.0), 6.87 (1 H, t, *J* 2.0), 6.80−6.75 (2 H, m), 6.72 (1 H, daq, *J* 8.0, 1.0), 6.72 (1 H, daq,

https://doi.org/10.1021/acsinfecdis.1c00231
ACS Infect. Dis. XXXX, XXX, XXX−XXX

J 8.9, 1.2), 5.53 (2 H, bs), 3.71 (3 H, s); δ_C (125.5 MHz; $CDCl_3$) 158.6 (d, $^3J_{CF}$ 10.2), 157.4 (d, $^1J_{CF}$ 247.8), 149.1, 140.6, 129.4, 128.8 (d, $^2J_{CF}$ 2.5), 117.4, 116.7 (d, $^3J_{CF}$ 13.4), 113.3, 111.2, 110.1 (d, $^4J_{CF}$ 3.1), 102.0 (d, $^2J_{CF}$ 23.7), 55.7; HRMS-ESI calcd for $C_{13}H_{14}FN_2O_3S^+$ $[M + H]^+$: 297.0704, found: 297.0702.

*3-Amino-N-(benzo[d][1,3]dioxol-5-yl)-benzenesulfonamide (**21**).* Method B. Yield: 98%; brown solid; mp 128−130 °C; δ_H (500 MHz; DMSO-d_6) 9.82 (1 H, s), 7.13 (1 H, t, *J* 7.9), 6.90 (1 H, t, *J* 2.0), 6.81 (1 H, daq, *J* 7.7, 0.9), 6.76 (1 H, d, *J* 8.4), 6.71 (1 H, daq, *J* 8.1, 1.0), 6.64 (1 H, d, *J* 2.1), 6.68 (1 H, dd, *J* 8.3, 2.1), 5.95 (2 H, s), 5.55 (2 H, bs); δ_C (125.5 MHz; DMSO-d_6) 149.2, 147.3, 144.1, 139.9, 131.8, 129.5, 117.5, 114.3, 113.3, 111.3, 108.42, 103.1, 101.2; HRMS-ESI calcd for $C_{13}H_{13}N_2O_4S^+$ $[M + H]^+$: 293.0591, found: 293.0581.

*3-Amino-N-(4-(difluoromethoxy)phenyl)-benzenesulfonamide (**22**).* Method B. Yield: 84%; white/pink solid; mp 102−104 °C; δ_H (500 MHz; DMSO-d_6) 10.18 (1 H, bs), 7.15 (1 H, t, *J* 7.9), 7.12 (2 H, d, *J* 9.1), 7.10 (1 H, t, $^2J_{HF}$ 76.3), 7.07 (2 H, d, *J* 9.1), 6.96−6.95 (1 H, m), 6.85 (1 H, daq, *J* 7.7, 0.9), 6.72 (1 H, daq, *J* 8.1, 1.0), 5.58 (2 H, bs); δ_C (125.5 MHz; DMSO-d_6) 149.4, 147.08 (t, $^3J_{CF}$ 3.2), 140.0, 135.2, 129.6, 121.5, 119.8, 117.6, 116.4 (t, $^1J_{CF}$ 257.6); HRMS-ESI calcd for $C_{13}H_{13}F_2N_2O_3S^+$ $[M + H]^+$: 315.0609, found: 315.0618.

*3-Amino-N-(4-(trifluoromethoxy)phenyl)-benzenesulfonamide (**23**).* Method B. Yield: 97%; light brown solid; mp 105−106 °C; δ_H (500 MHz; DMSO-d_6) 10.37 (1 H, bs), 7.25 (1 H, d, *J* 8.5), 7.18−7.13 (3 H, m), 6.96 (1 H, t, *J* 2.0), 6.86 (2 H, daq, *J* 8.1, 0.9), 6.72 (2 H, daq, *J* 8.1, 1.0), 5.59 (2 H, bs); δ_C (125.5 MHz; DMSO-d_6) 149.5, 144.15 (q, $^3J_{CF}$ 1.9), 139.9, 137.3, 129.7, 122.0, 120.8, 120.1 (q, $^1J_{CF}$ 255.9), 117.8, 117.0, 113.2, 111.0; HRMS-ESI calcd for $C_{13}H_{12}F_3N_2O_3S^+$ $[M + H]^+$: 333.0515, found: 333.0523.

*3-Amino-4-chloro-N-(4-methoxyphenyl)-benzenesulfonamide (**24**).* Method B. Yield: 87%; off white thick oil; δ_H (500 MHz; $CDCl_3$) 7.26 (1 H, d, *J* 8.3), 7.12 (1 H, d, *J* 2.2), 6.99 (2 H, d, *J* 8.9), 6.96 (1 H, dd, *J* 8.4, 2.2), 6.77 (2 H, d, *J* 9.0), 6.63, (1 H, bs), 4.27, (2 H, bs), 3.76 (3 H, s); δ_C (125.5 MHz; $CDCl_3$) 158.1, 143.5, 138.2, 129.8, 128.5, 125.7, 123.5, 117.4, 114.5, 113.8, 55.4; HRMS-ESI calcd for $C_{13}H_{14}ClN_2O_3S^+$ $[M + H]^+$: 313.0408, found: 313.0412.

*3-Amino-4-chloro-N-(2-fluorophenyl)-benzenesulfonamide (**25**).* Method B. Yield: 87%; off white solid; mp 119−121 °C; δ_H (500 MHz; DMSO-d_6) 10.08 (1 H, bs), 7.35 (1 H, d, *J* 8.3), 7.22 (1 H, at, *J* 8.0), 7.20−7.10 (4 H, m), 6.83 (1 H, dd, *J* 8.3, 2.2), 5.84 (2 H, bs); δ_C (125.5 MHz; DMSO-d_6) 155.7 (d, $^1J_{CF}$ 247.3), 154.7, 139.5, 129.7, 127.15 (d, $^2J_{CF}$ 7.4), 126.4 (d, $^4J_{CF}$ 0.6), 124.6 (d, $^3J_{CF}$ 3.8), 124.5, 120.7, 116.0 (d, $^2J_{CF}$ 19.8), 114.0, 112.8; HRMS-ESI calcd for $C_{12}H_{11}ClFN_2O_2S^+$ $[M + H]^+$: 301.0208, found: 301.0209.

*3-Amino-4-chloro-N-(2-fluoro-4-methoxyphenyl)-benzenesulfonamide (**26**).* Method B. Yield: 94%; off white solid; mp 97−99; δ_H (500 MHz; $CDCl_3$) 7.42 (1 H, t, *J* 9.0), 7.27 (1 H, d, *J* 5.7), 7.11 (1 H, d, *J* 2.2), 6.96 (1 H, dd, *J* 8.4, 2.2), 6.66 (1 H, daq, *J* 9.0, 1.0), 6.53 (1 H, dd, *J* 11.8, 2.8), 6.46 (1 H, bs), 4.26 (2 H, bs), 3.76 (3 H, s); δ_C (125.5 MHz; $CDCl_3$) 158.93 (d, $^3J_{CF}$ 10.2), 156.1 (d, $^1J_{CF}$ 246.1), 143.4, 138.1, 129.9, 127.04 (d, $^2J_{CF}$ 1.9), 123.7, 117.0, 116.4 (d, $^3J_{CF}$ 13.3), 113.7, 110.14 (d, $^4J_{CF}$ 3.3), 101.9 (d, $^2J_{CF}$ 23.3), 55.7; HRMS-ESI calcd for $C_{13}H_{13}ClFN_2O_3S^+$ $[M + H]^+$: 331.0314, found: 331.0316.

*3-Amino-N-(benzo[d][1,3]dioxol-5-yl)-4-chlorobenzenesulfonamide (**27**).* Method B. Yield: 86%; light brown solid; mp 131−132 °C; δ_H (500 MHz; DMSO-d_6) 9.92 (1 H, bs), 7.34 (1 H, d, *J* 6.3), 7.127 (1 H, d, *J* 2.2), 6.81 (1 H, dd, *J* 8.3, 2.2), 6.77 (1 H, d, *J* 8.3), 6.648 (1 H, d, *J* 2.1), 6.476 (1 H, dd, *J* 8.3, 2.3), 5.96 (2 H, s), 5.84 (2 H, bs); δ_C (125.5 MHz; DMSO-d_6) 147.4, 145.1, 144.4, 138.7, 131.5, 129.7, 120.7, 114.7, 114.1, 113.0, 108.3, 103.4, 101.3; HRMS-ESI calcd for $C_{13}H_{12}ClN_2O_4S^+$ $[M + H]^+$: 327.0201, found: 327.0204.

*3-Amino-4-chloro-N-(4-(difluoromethoxy)phenyl)-benzenesulfonamide (**28**).* Method B. Yield: 78%; light brown solid; mp 109−111 °C; δ_H (500 MHz; DMSO-d_6) 10.26 (1 H, bs), 7.35 (1 H, d, *J* 8.41), 7.18 (1 H, d, *J* 2.2), 7.12−7.07 (4 H, m), 7.10 (1 H, t, $^2J_{HF}$ 74.2), 6.85 (1 H, dd, *J* 8.3, 2.2), 5.87 (2 H, bs); δ_C (125.5 MHz; DMSO-d_6) 147.4 (t, $^3J_{CF}$ 3.2), 145.3, 138.7, 134.8, 129.8, 121.9, 120.9, 116.4 (t, $^1J_{CF}$ 257.7), 114.0, 12.8; HRMS-ESI calcd for $C_{13}H_{13}ClF_2N_2O_3S^+$ $[M + H]^+$: 349.0220, found: 349.0222.

*3-Amino-4-chloro-N-(4-(trifluoromethoxy)phenyl)-benzenesulfonamide (**29**).* Method B. Yield: 90%; light brown solid; mp 123−126 °C; δ_H (500 MHz; DMSO-d_6) 10.47 (1 H, bs), 7.36 (1 H, d, *J* 8.4), 7.28 (2 H, d, *J* 8.4), 7.21 (1 H, d, *J* 2.2), 7.17 (2 H, d, *J* 9.1), 6.87 (1 H, dd, *J* 8.4, 2.3), 5.89 (2 H, bs); δ_C (125.5 MHz; DMSO-d_6) 145.3, 144.38 (q, $^3J_{CF}$ 1.9), 138.7, 137.0, 129.9, 122.1, 121.3, 121.0, 120.3 (q, $^1J_{CF}$ 256.0), 113.9, 112.7; HRMS-ESI calcd for $C_{13}H_{11}ClF_3N_2O_3S^+$ $[M + H]^+$: 367.0126, found: 367.0116.

3,5-Difluorobenzoyl Chloride. 3,5-Difluorobenzoic acid (1.0 g, 6.32 mmol) was dissolved in a mixture of chloroform (1M; 6.3 mL) and thionyl chloride (1.0 mL, 14.53 mmol), and the mixture was heated at reflux for 8 h under an argon atmosphere. While removing the solvent and excess reagent in vacuo, the product was collected in the antisplash bulb as a colorless liquid, which was stored in a vial, with the latter being kept in a molecular sieve containing jar at 5−8 °C. The acyl chloride easily hydrolyzed back to the acid upon contact with humid air: δ_H (500 MHz; $CDCl_3$) 7.68 (2 H, m); 7.16 (1 H, tt, *J* 8.3, 2.4); δ_C (125.5 MHz; $CDCl_3$) 166.4, 162.8 (dd, $^{1,3}J_{CF2}$ 252.5, 11.9), 136.2 (at, $^3J_{CF2}$ 9.0), 114.25 (dd, $^{2,4}J_{CF2}$ 20.9, 7.1), 110.8 (at, $^3J_{CF2}$ 25.2).

*3,5-Difluoro-N-(3-(N-(4-methoxyphenyl)sulfamoyl)-phenyl)benzamide (**1**).* Method C. Purification: the crude solid was recrystallized from a 9:1 chloroform/ethyl acetate mixture; yield: 35%; HPLC purity: 98%; white fluffy solid; mp 205−206 °C; δ_H (600 MHz; DMSO-d_6) 10.61 (1 H, bs), 10.01 (1 H, s), 8.29 (1 H, t, *J* 1.9), 7.95 (1 H, dd, *J* 8.2, 1.2), 7.71−7.68 (2 H, m), 7.553 (1 H, tt, *J* 9.2, 2.3), 7.558 (1 H, t, *J* 8.1), 7.43 (1 H, d, *J* 8.3), 7.00 (1 H, d, *J* 9.0), 6.81 (1 H, d, *J* 9.0), 3.66 (3 H, s); δ_C (150 MHz; DMSO-d_6) 163.16, 162.2 (dd, $^{1,3}J_{CF2}$ 247.5, 12.8), 156.5, 140.1, 139.2, 137.8 (t, $^3J_{CF2}$ 8.6), 130.0, 129.6, 124.0, 123.5, 122.1, 118.3, 114.3, 111.25 (dd, $^{2,4}J_{CF2}$ 20.4, 6.6), 107.3 (t, $^2J_{CF2}$ 25.9), 55.1; HRMS-ESI calcd for $C_{20}H_{20}F_2N_3O_4S^+$ $[M + NH_4]^+$: 436.1137, found: 436.1133.

*3,5-Difluoro-N-(3-(N-(2-fluorophenyl)sulfamoyl)phenyl)-benzamide (**30**).* Method C. Purification: the crude solid was suspended in chloroform, allowing for the excess benzoyl chloride to be removed; yield: 30%; HPLC purity: >99%; white solid; mp 237−238 °C; δ_H (500 MHz; DMSO-d_6) 10.62 (1 H, bs), 10.23 (1 H, bs), 8.30 (1 H, t, *J* 1.9), 8.00 (1 H, dat, *J* 8.2, 0.9), 7.69 (1 H, dd, *J* 8.1, 2.2), 7.58−7.53 (2 H, m), 7.47 (1 H, d, *J* 8.3), 7.25 (1 H, dt, *J* 8.0, 1.7), 7.22−7.11 (3 H, m); δ_C (125.5 MHz; DMSO-d_6) 163.17, 162.20 (dd, $^{1,3}J_{CF2}$ 247.6,

https://doi.org/10.1021/acsinfecdis.1c00231
ACS Infect. Dis. XXXX, XXX, XXX−XXX

12.8), 155.7 (d, $^{1}J_{CF}$ 247.4), 140.6, 139.2, 137.78 (t, $^{3}J_{CF2}$ 7.7), 129.7, 127.43 (d, $^{2}J_{CF}$ 7.3), 126.6, 124.69 (d, $^{4}J_{CF}$ 3.9), 124.2, 124.26 (d, $^{3}J_{CF}$ 12.9), 121.9, 118.1, 116.06 (d, $^{2}J_{CF}$ 9.7), 111.25 (dd, $^{2,4}J_{CF2}$ 20.6, 6.6), 107.35 (t, $^{2}J_{CF2}$ 26.7); HRMS-ESI calcd for $C_{19}H_{14}F_3N_2O_3S^+$ $[M + H]^+$: 407.0672, found: 407.0673.

*3,5-Difluoro-N-(3-(N-(2-fluoro-4-methoxyphenyl)-sulfamoyl)phenyl)benzamide (**31**).* Method C. Purification: the crude solid was recrystallized from a 9:1 chloroform/ethyl acetate mixture; yield: 35%; HPLC purity: 97%; white solid; mp 218−220 °C; δ_H (500 MHz; DMSO-d_6) 10.61 (1 H, bs), 9.88 (1 H, bs), 8.24 (1 H, s), 8.03 (1 H, dd, *J* 8.1, 1.1), 6.70 (2 H, d, *J* 6.0), 7.57−7.53 (2 H, m), 7.42 (1 H, d, *J* 7.9), 7.07 (1 H, t, *J* 9.0), 6.80 (1 H, dd, *J* 12.0, 2.7), 6.72 (1 H, dd, *J* 8.9, 2.4), 3.71 (3 H, s); δ_C (125.5 MHz; DMSO-d_6) 163.14, 162.20 (dd, $^{1,3}J_{CF2}$ 247.4, 12.7), 158.9 (d, $^{3}J_{CF}$ 10.2), 157.6 (d, $^{1}J_{CF}$ 247.9), 140.7, 139.1, 137.8 (t, $^{3}J_{CF2}$ 8.6), 129.6, 129.35 (d, $^{2}J_{CF}$ 2.3), 124.0, 122.0, 116.16 (d, $^{3}J_{CF}$ 13.5), 111.24 (dd, $^{2,4}J_{CF2}$ 20.4, 6.7), 110.27 (d, $^{4}J_{CF}$ 2.9), 107.3 (t, $^{2}J_{CF2}$ 26.0), 102.06 (d, $^{2}J_{CF}$ 23.8), 55.7; HRMS-ESI calcd for $C_{20}H_{16}F_3N_2O_4S^+$ $[M + H]^+$: 437.0777, found: 437.0783.

*N-(3-(N-(Benzo[d][1,3]dioxol-5-yl)sulfamoyl)phenyl)-3,5-difluorobenzamide (**32**).* Method C. Purification: the crude oil was taken up in ethyl acetate (0.1 mL), followed by chloroform (1.9 mL), and the precipitate was isolated by filtration; yield: 62%; HPLC purity: 98%; white fluffy solid; mp 196−198 °C; δ_H (500 MHz; DMSO-d_6) 10.61 (1 H, bs), 10.08 (1 H, s), 8.29 (1 H, t, *J* 1.9), 7.96 (1 H, daq, *J* 8.2, 1.0), 7.71−7.67 (2 H, m), 7.56−7.51 (2 H, m), 7.46 (1 H, daq, *J* 7.9, 1.0), 6.76 (1 H, d, *J* 8.3), 6.67 (1 H, d, *J* 2.1), 6.51 (1 H, dd, *J* 8.4, 2.2), 5.95 (2 H, s); δ_C (125.5 MHz; DMSO-d_6) 163.21 (t, $^{4}J_{CF2}$ 3.0), 162.22 (dd, $^{1,3}J_{CF2}$ 247.5, 12.6), 147.4, 144.5, 139.9, 139.2, 137.81 (t, $^{3}J_{CF2}$ 8.6), 131.3, 129.7, 124.1, 122.1, 118.4, 114.8, 111.27 (dd, $^{2,4}J_{CF2}$ 20.3, 6.7), 108.3, 107.36 (t, $^{2}J_{CF2}$ 25.9), 103.5, 101.3; HRMS-ESI calcd for $C_{20}H_{18}F_2N_2O_5S^+$ $[M + NH_4]^+$: 450.0930, found: 450.0925.

*N-(3-(N-(4-(Difluoromethoxy)phenyl)sulfamoyl)phenyl)-3,5-difluorobenzamide (**33**).* Method C. Purification: the crude oil was taken up in ethyl acetate (0.1 mL), followed by chloroform (1.9 mL), and the precipitate was isolated by filtration; yield: 60%; HPLC purity: 98%; white solid; mp 199−201 °C; δ_H (500 MHz; DMSO-d_6) 10.62 (1 H, bs), 10.42 (1 H, bs), 8.35 (1 H, t, *J* 1.9), 7.95 (1 H, daq, *J* 8.0, 1.0), 7.70−7.67 (2 H, m), 7.57−7.49 (3 H, m), 7.14 (2 H, d, *J* 9.1), 7.09 (1 H, t, $^{2}J_{HF}$ 74.1), 7.08 (2 H, d, *J* 9.0); δ_C (125.5 MHz; DMSO-d_6) 163.24 (t, $^{4}J_{CF2}$ 3.0), 162.2 (dd, $^{1,3}J_{CF2}$ 247.4, 12.8), 147.38 (t, $^{3}J_{CF2}$ 3.3), 140.0, 139.4, 137.8 (t, $^{3}J_{CF2}$ 8.6), 134.7, 129.8, 124.3, 122.0, 119.9, 118.25, 116.4 (t, $^{1}J_{CF2}$ 257.8), 111.26 (dd, $^{2,4}J_{CF2}$ 20.3, 6.6), 107.38 (t, $^{2}J_{CF2}$ 25.8); HRMS-ESI calcd for $C_{20}H_{18}F_4N_3O_4S^+$ $[M + NH_4]^+$: 472.0949, found: 472.0959.

*3,5-Difluoro-N-(3-(N-(4-(trifluoromethoxy)phenyl)-sulfamoyl)phenyl)benzamide (**34**).* Method C. Purification: the crude oil was taken up in ethyl acetate (0.1 mL), followed by chloroform (1.9 mL), and the precipitate was isolated by filtration; yield: 78%; HPLC purity: > 99%; white solid; mp 208−210 °C; δ_H (500 MHz; DMSO-d_6) 10.63 (2 H, bs), 8.38 (1 H, t, *J* 1.8), 7.95 (1 H, daq, *J* 8.0, 1.1), 7.71−7.66 (2 H, m), 7.58−7.51 (3 H, m), 7.26 (2 H, d, *J* 9.6), 7.20 (2 H, d, *J* 9.1); δ_C (125.5 MHz; DMSO-d_6) 163.23 (t, $^{4}J_{CF2}$ 3.0), 162.16 (dd, $^{1,3}J_{CF2}$ 247.4, 12.6), 144.46 (q, $^{3}J_{CF3}$ 2.2), 139.9, 139.4, 137.8 (t, $^{3}J_{CF2}$ 8.6), 136.9, 129.9, 124.4, 122.1, 122.0, 121.4, 120.0 (q, $^{1}J_{CF3}$ 256.0), 118.2, 111.25 (dd, $^{2,4}J_{CF2}$ 20.4, 6.6), 107.37 (t, $^{2}J_{CF2}$ 26.0); HRMS-ESI calcd for $C_{20}H_{17}F_5N_3O_4S^+$ $[M + NH_4]^+$: 490.0854, found: 490.0869.

*N-((3-Amino-4-chlorophenyl)sulfonyl)-3,5-difluoro-N-(4-methoxyphenyl)-benzamide (**35**).* Method C. Purification: the crude oil was purified on silica gel eluting with 100% chloroform; yield: 25%; HPLC purity: 95%; green waxy solid; δ_H (500 MHz; $CDCl_3$) 7.42 (1 H, d, *J* 2.1), 7.36 (1 H, d, *J* 8.4), 7.11 (1 H, dd, *J* 8.4, 2.1), 7.06−7.03 (2 H, m), 6.98−6.93 (2 H, m), 6.82−6.79 (2 H, m), 6.75 (1 H, tt, *J* 8.5, 2.3), 4.35 (2 H, bs), 3.78 (3 H, s); δ_C (125.5 MHz; $CDCl_3$) 167.31 (at, $^{4}J_{CF2}$ 3.1), 162.23 (dd, $^{1,3}J_{CF2}$ 251.1, 12.1), 160.3, 143.3, 136.84 (at, $^{3}J_{CF2}$ 8.9), 136.7, 131.3, 129.6, 128.8, 124.7, 118.9, 116.0, 114.6, 111.45 (dd, $^{2,4}J_{CF2}$ 20.7, 6.9), 107.21 (at, $^{2}J_{CF2}$ 25.2), 55.5; HRMS (ESI) calcd for $C_{20}H_{16}ClF_2N_2O_2S^+$ $[M + H]^+$: 453.0482, found: 452.9969.

*N-((3-Amino-4-chlorophenyl)sulfonyl)-3,5-difluoro-N-(2-fluoro-4-methoxy-phenyl)benzamide (**36**).* Method C. Purification: the crude oil was purified on silica gel eluting with hexane/chloroform/ether (5:4:1 to 4.5:3.5:2); yield: 52%; HPLC purity: >99%; off-white powder; δ_H (500 MHz; $CDCl_3$) 7.49 (1 H, d, *J* 2.2), 7.38 (1 H, d, *J* 8.4), 7.23 (1 H, t, *J* 8.8), 7.20 (1 H, dd, *J* 8.4, 2.1), 6.94−6.92 (2 H, m), 6.77 (1 H, tt, *J* 8.6, 2.3), 6.68 (1 H, dd, *J* 8.9, 2.8), 6.55 (1 H, dd, *J* 11.6, 2.8), 4.36 (2 H, bs), 3.78 (3 H, s); δ_C (125.5 MHz; $CDCl_3$) 167.1 (at, $^{4}J_{CF2}$ 3.0), 162.25 (dd, $^{1,3}J_{CF2}$ 251.3, 12.0), 162.20 (d, $^{2}J_{CF}$ 10.8), 159.0 (d, $^{1}J_{CF}$ 251.7), 143.3, 137.0, 136.56 (at, $^{3}J_{CF2}$ 8.8), 132.5 (d, $^{4}J_{CF}$ 1.2), 129.7, 124.9, 118.8, 111.63 (d, $^{3}J_{CF}$ 3.2), 116.0, 111.58 (dd, $^{2,4}J_{CF2}$ 20.8, 7.0), 110.76 (d, $^{3}J_{CF}$ 2.9), 107.16 (at, $^{2}J_{CF2}$ 25.1), 102.32 (d, $^{2}J_{CF}$ 23.5), 55.8; HRMS (ESI) calcd for $C_{20}H_{15}ClF_3N_2O_4S^+$ $[M + H]^+$: 471.0388, found: 471.0392.

*N-(2-Chloro-5-(N-(2-fluorophenyl)sulfamoyl)phenyl)-3,5-difluorobenzamide (**37**).* Method C. Purification: the crude oil was purified on silica gel eluting with hexane/ethyl acetate (4:1 to 7:3); yield: 20%; HPLC purity: > 99%; white solid; mp 140−141 °C; δ_H (500 MHz; DMSO-d_6) 9.06 (1 H, bs), 8.34 (1 H, bs), 7.62 (1 H, dt, *J* 7.9, 1.9), 7.49 (2 H, s), 7.43−7.38 (2 H, m), 7.15−7.03 (3 H, m), 7.01−6.97 (2 H, m); δ_C (125.5 MHz; DMSO-d_6) 163.20 (dd, $^{1,3}J_{CF2}$ 252.2, 12.1), 162.7 (t, $^{4}J_{CF2}$ 3.1), 154.1 (d, $^{1}J_{CF}$ 245.2), 138.9, 137.06 (t, $^{3}J_{CF2}$ 8.3), 134.9, 129.6, 127.8, 126.54 (d, $^{2}J_{CF}$ 7.5), 124.92 (d, $^{4}J_{CF}$ 1.8), 124.12 (d, $^{2}J_{CF}$ 12.4), 123.57 (d, $^{3}J_{CF}$ 11.3), 120.0, 115.54 (d, $^{2}J_{CF}$ 19.4), 110.47 (dd, $^{2,4}J_{CF2}$ 20.0, 7.0), 108.0 (t, $^{2}J_{CF2}$ 25.2); HRMS-ESI calcd for $C_{19}H_{16}ClF_3N_3O_3S^+$ $[M + NH_4]^+$: 458.0548, found: 458.0542.

*N-(5-(N-(Benzo[d][1,3]dioxol-5-yl)sulfamoyl)-2-chlorophenyl)-3,5-difluoro-benzamide (**38**).* Method C. Purification: the crude oil was purified on silica gel eluting with chloroform/ethyl acetate (9:1); yield: 53%; HPLC purity: >99%; white fluffy solid; mp 186−187 °C; δ_H (500 MHz; DMSO-d_6) 8.98 (1 H, d, *J* 2.1), 8.97 (1 H, bs), 7.47 (1 H, d, *J* 8.4), 7.43 (1 H, dd, *J* 8.4, 2.1), 7.41−7.37 (2 H, m), 7.12 (1 H, s), 7.05 (1 H, tt, *J* 8.5, 2.3), 6.74 (1 H, d, *J* 2.1), 6.64 (1 H, d, *J* 8.3), 6.54 (1 H, dd, *J* 8.3, 2.2), 5.93 (2 H, s); δ_C (125.5 MHz; DMSO-d_6) 163.20 (dd, $^{1,3}J_{CF2}$ 252.1, 12.1), 163.0 (t, $^{4}J_{CF2}$ 3.0), 148.1, 146.2, 138.1, 137.06 (t, $^{3}J_{CF2}$ 8.3), 134.7, 129.7, 129.4, 127.9, 124.2, 120.2, 117.3, 110.53 (dd, $^{2,4}J_{CF2}$ 20.1, 7.2), 108.3, 108.1 (t, $^{2}J_{CF2}$ 25.2), 105.8, 101.6; HRMS-ESI calcd for $C_{20}H_{17}ClF_2N_3O_5S^+$ $[M + NH_4]^+$: 484.0540, found: 484.0539.

*N-(2-Chloro-5-(N-(4-(difluoromethoxy)phenyl)sulfamoyl)-phenyl)-3,5-difluorobenzamide (**39**).* Method C. Purification: the crude oil was purified on silica gel eluting with chloroform/

https://doi.org/10.1021/acsinfecdis.1c00231
ACS Infect. Dis. XXXX, XXX, XXX−XXX

ethyl acetate (93:7); yield: 25%; HPLC purity: >99%; off white solid; mp 161−163 °C; δ_H (500 MHz; DMSO-d_6) 8.98 (1 H, bs), 8.37 (1 H, bs), 7.49−7.46 (3 H, m), 7.40−7.35 (2 H, m), 7.16 (2 H, d, *J* 9.1), 7.05 (1 H, tt, *J* 8.5, 2.3), 7.00 (2 H, d, *J* 9.1), 6.44 (1 H, t, $^2J_{HF}$ 74.1); δ_C (125.5 MHz; DMSO-d_6) 163.21 (dd, $^{1,3}J_{CF2}$ 252.3, 12.1), 163.09 (t, $^4J_{CF2}$ 3.1), 148.88 (t, $^3J_{CF2}$ 2.9), 138.7, 136.99 (t, $^3J_{CF2}$ 8.4), 134.8, 133.4, 129.7, 128.1, 124.1, 124.0, 120.7, 120.2, 115.8 (t, $^1J_{CF2}$ 260.6), 111.52 (dd, $^{2,4}J_{CF2}$ 20.2, 7.1), 108.16 (t, $^2J_{CF2}$ 25.2); HRMS-ESI calcd for $C_{20}H_{17}ClF_4N_3O_4S^+$ $[M + NH_4]^+$: 506.0559, found: 506.0551.

*N-(2-Chloro-5-(N-(4-(trifluoromethoxy)phenyl)sulfamoyl)-phenyl)-3,5-difluorobenzamide (**40**).* Method C. Purification: the crude oil was purified on silica gel eluting with chloroform/ethyl acetate (93:7); yield: 14%; HPLC purity: >99%; off white solid; mp 169−171 °C; δ_H (500 MHz; DMSO-d_6) 9.05 (1 H, s), 8.38 (1 H, bs), 7.49−7.47 (3 H, m), 7.41−7.35 (2 H, m), 7.20 (2 H, d, *J* 9.0), 7.10 (2 H, d, *J* 8.5), 7.06 (1 H, tt, *J* 8.4, 2.3); δ_C (125.5 MHz; DMSO-d_6) 163.23 (dd, $^{1,3}J_{CF2}$ 252.4, 12.2), 163.09 (t, $^4J_{CF2}$ 3.1), 146.72 (q, $^3J_{CF3}$ 1.9), 138.7, 136.96 (t, $^3J_{CF2}$ 8.3), 134.8, 129.7, 128.1, 124.0, 123.4, 123.3, 122.1, 120.36 (q, $^1J_{CF3}$ 257.3), 120.0, 111.52 (dd, $^{2,4}J_{CF2}$ 20.3, 7.1), 108.2 (t, $^2J_{CF2}$ 25.2); HRMS-ESI calcd for $C_{20}H_{16}ClF_5N_3O_4S^+$ $[M + NH_4]^+$: 524.0465, found: 524.0471.

*N-(3-(N-(2-Fluorophenyl)sulfamoyl)phenyl)pyrazine-2-carboxamide (**41**).* To a solution of aniline **19** (60 mg, 0.23 mmol), pyrazine-2-carboxylic acid (56 mg, 0.46 mmol), EDCI (65 mg, 0.34 mmol), and HOBt (52 mg, 0.34 mmol) in anhydrous DMF (1.1 mL, 0.2M) at 0 °C was added triethylamine (94 μL, 0.68 mmol) dropwise under an argon atmosphere. The reaction mixture was left to stir overnight at room temperature, diluted with ethyl acetate (3 mL), and filtered. The resulting solution was washed with brine (2 × 5 mL), 1 M HCl (5 mL), saturated aqueous $NaHCO_3$ (2 × 5 mL), brine (5 mL), dried over $MgSO_4$, and filtered, and the solvent was removed in vacuo. The crude product was purified on silica gel eluting with hexane/ethyl acetate (1:1) to yield the *title product* (44 mg; 52%) as white solid; HPLC purity: 97%; mp 205−206 °C; δ_H (500 MHz; DMSO-d_6) 11.09 (1 H, bs), 10.24 (1 H, bs), 9.31 (1 H, d, *J* 1.4), 8.95 (1 H, d, *J* 2.5), 8.25 (1 H, aq, *J* 1.3), 8.55 (1 H, at, *J* 1.7), 8.07 (1 H, dd, *J* 8.2, 1.0), 7.56 (1 H, t, *J* 8.0), 7.48 (1 H, d, *J* 8.1), 7.27 (1 H, dt, *J* 1.4, 8.0), 7.21−7.11 (3 H, m); δ_C (125.5 MHz; DMSO-d_6) 162.2, 155.6 (d, $^1J_{CF}$ 247.4), 147.9, 144.8, 144.2, 143.3, 140.6, 138.8, 129.6, 127.3 (d, $^2J_{CF}$ 7.4), 126.5, 124.66 (d, $^4J_{CF}$ 3.8), 124.5, 124.32 (d, $^3J_{CF}$ 12.8), 122.1, 118.4, 116.03 (d, $^2J_{CF}$ 19.3); HRMS-ESI calcd for $C_{17}H_{14}FN_4O_3S^+$ $[M + H]^+$: 373.0765, found: 373.0767.

*3-Fluoro-4-methoxy-N-(3-(N-(4-methoxyphenyl)-sulfamoyl)phenyl)benza-mide (**42**).* To a solution of aniline **18** (72 mg, 0.26 mmol), 3-fluoro-4-methoxy-benzoyl chloride (108 mg, 0.56 mmol) and DMAP (16 mg, 0.14 mmol) in anhydrous acetonitrile (1.3 mL, 0.2M) at room temperature was added *N*-methylmorpholine (85 μL; 0.78 mmol; 3.0 equiv) dropwise under an argon atmosphere. The reaction mixture was left to stir overnight at room temperature, and the solvent was removed in vacuo. The crude oil was diluted with ethyl acetate (2 mL), washed with 1 M HCl (2 mL), saturated aqueous $NaHCO_3$ (2 mL), brine (2 mL), dried over $MgSO_4$, and filtered and the solvent was removed in vacuo. Purification: the crude solid was recrystallized several times from a 9:1 methanol/acetone mixture to yield the *title product* (18 mg; 16%) as a white solid; HPLC purity: 95%; mp 202−203 °C; δ_H (500 MHz; acetone-d_6) 9.68 (1 H, bs), 8.78 (1 H, bs), 8.35 (1 H, s), 8.00 (1 H, daq, *J* 7.9, 1.1), 7.87 (1 H, daq, *J* 8.6, 1.0), 7.81 (1 H, dd, *J* 12.2, 2.1), 7.46 (1 H, t, *J* 7.9), 7.43 (1 H, dt, *J* 8.1, 0.9), 7.27 (1 H, t, *J* 8.6), 7.13 (2 H, d, *J* 9.0), 6.81 (2 H, d, *J* 9.0), 3.97 (3 H, s), 3.72 (3 H, s); δ_C (125.5 MHz; acetone-d_6) 164.03 (d, $^4J_{CF}$ 2.2), 157.5, 151.6 (d, $^1J_{CF}$ 245.4), 150.83 (d, $^2J_{CF}$ 10.7), 140.6, 140.0, 130.2, 129.2, 127.16 (d, $^3J_{CF}$ 5.6), 124.61 (d, $^3J_{CF}$ 3.4), 124.3, 123.6, 122.1, 118.4, 115.16 (d, $^2J_{CF}$ 19.9), 114.2, 113.01 (d, $^4J_{CF}$ 2.0), 55.8, 54.7; HRMS-ESI calcd for $C_{21}H_{23}FN_3O_5S^+$ $[M + NH_4]^+$: 448.1337, found: 448.1348.

*N-(2-Fluorophenyl)-3-((4-methoxybenzyl)amino)-benzenesulfonamide (**43**).* To a solution of aniline **19** (50 mg, 0.19 mmol), 4-methoxybenzaldehyde (31 mg, 0.23 mmol), and acetic acid (13 μL, 0.23 mmol) were added crushed 3 Å molecular sieves (50 mg) in anhydrous dichloromethane (1.9 mL, 0.1M). After stirring at room temperature for 30 min, sodium triacetoxyborohydride (80 mg, 0.38 mmol) was added and the reaction mixture stirred for another 16 h, upon which time it was diluted with chloroform (3 mL) and centrifuged to remove the molecular sieves. After washing with water (3 mL), the organic layer was dried over $MgSO_4$ and filtered and the solvent was removed in vacuo. The crude product was purified on silica gel eluting with 100% chloroform to yield the *title product* (46 mg; 63%) as an off white solid; HPLC purity: 97%; mp 109−110 °C; δ_H (500 MHz; $CDCl_3$) 7.57−7.54 (1 H, m), 7.21 (2 H, d, *J* 8.6), 7.17 (1 H, t, *J* 8.0), 7.07−7.02 (3 H, m), 6.99−6.95 (2 H, m), 6.87 (2 H, d, *J* 8.7), 6.73−6.69 (2 H, m), 4.18 (3 H, bs), 3.80 (3 H, s); δ_C (125.5 MHz; $CDCl_3$) 159.0, 153.8 (d, $^1J_{CF}$ 244.3), 148.4, 139.6, 130.1, 129.8, 128.8, 125.81 (d, $^3J_{CF}$ 7.4), 124.86 (d, $^2J_{CF}$ 12.3), 124.66 (d, $^3J_{CF}$ 3.9), 122.9, 119.6, 117.4, 115.6, 115.32 (d, $^2J_{CF}$ 19.5), 114.1, 110.2, 55.3, 47.4; HRMS-ESI calcd for $C_{20}H_{20}FN_2O_3S^+$ $[M + H]^+$: 387.1173, found: 387.1164.

■ ASSOCIATED CONTENT

Supporting Information

The Supporting Information is available free of charge at https://pubs.acs.org/doi/10.1021/acsinfecdis.1c00231.

Sequence alignment of eukaryotic malic enzymes; SEC and oligomeric state analysis of *T. cruzi* malic enzymes; superposition of malic enzymes from *T. cruzi* (cytosolic isoform) with human mitochondrial isoform (HsME2); activity of previously reported TcMEc sulfonamide inhibitors over intracellular form of *T. cruzi*; ^{1}H and ^{13}C NMR spectra for all compounds synthesized (PDF)

■ AUTHOR INFORMATION

Corresponding Authors

Artur T. Cordeiro − *Brazilian Biosciences National Laboratory, Brazilian Center for Research in Energy and Materials, Campinas, SP 13083-970, Brazil; Faculty of Pharmaceutic Sciences, University of Campinas, Campinas, SP 13083-871, Brazil;* orcid.org/0000-0002-5676-2456; Email: artur.cordeiro@lnbio.cnpem.br

Marjorie Bruder − *Brazilian Biosciences National Laboratory, Brazilian Center for Research in Energy and Materials, Campinas, SP 13083-970, Brazil;* orcid.org/0000-0003-4236-848X; Email: marjorie.bruder@lnbio.cnpem.br

https://doi.org/10.1021/acsinfecdis.1c00231
ACS Infect. Dis. XXXX, XXX, XXX−XXX

Authors

Gustavo F. Mercaldi − *Brazilian Biosciences National Laboratory, Brazilian Center for Research in Energy and Materials, Campinas, SP 13083-970, Brazil*

Amanda G. Eufrásio − *Brazilian Biosciences National Laboratory, Brazilian Center for Research in Energy and Materials, Campinas, SP 13083-970, Brazil; Faculty of Pharmaceutic Sciences, University of Campinas, Campinas, SP 13083-871, Brazil*

Americo T. Ranzani − *Brazilian Biosciences National Laboratory, Brazilian Center for Research in Energy and Materials, Campinas, SP 13083-970, Brazil; Institute of Biology, University of Campinas, Campinas, SP 13083-970, Brazil*

Jessica do Nascimento Faria − *Brazilian Biosciences National Laboratory, Brazilian Center for Research in Energy and Materials, Campinas, SP 13083-970, Brazil*

Sabrina G. R. Mota − *Brazilian Biosciences National Laboratory, Brazilian Center for Research in Energy and Materials, Campinas, SP 13083-970, Brazil; Institute of Biology, University of Campinas, Campinas, SP 13083-970, Brazil*

Michelle Fagundes − *Brazilian Biosciences National Laboratory, Brazilian Center for Research in Energy and Materials, Campinas, SP 13083-970, Brazil*

Complete contact information is available at: https://pubs.acs.org/10.1021/acsinfecdis.1c00231

Author Contributions

‖G.F.M and A.E.G contributed equally to this work.

Notes

The authors declare no competing financial interest.

Structures of TcMEc were obtained in a ligand free form (PDB 7MF4) and in complexes with compounds **1** (PDB 6W29); **31** (PDB 6W2N); **33** (PDB 6W56); **34** (PDB 6W59); **39** (PDB 6W57); **40** (PDB 6W53); and **41** (PDB 6W49). Atomic coordinates and experimental data are available at Protein Data Bank.

■ ACKNOWLEDGMENTS

Authors thank GSK and Open Lab Foundation (Tres Cantos, Spain) for supplying the GSK Chagas box and performing the phenotypic assays that generated the data present in Table S1 in the Supporting Information. This study was supported by the São Paulo Research Foundation (FAPESP) (Grants 2013/03983-5 and 2018/22202-8) and by the Coordination for the Improvement of Higher Education Personnel (CAPES) (Grant 7775/2014-98). S.G.R.M. (Process No. 2014/15590-0 and 2016/19141-1) and A.T.R. (Process No. 2012/23682-7 and 2015/03336-5) were recipients of FAPESP fellowships. A.G.E. was recipient of FAPESP (2017/00674-2) and CAPES (88887.480232/2020-00) fellowships. The authors also thank the I03 beamline from the Diamond Light Source and the CNPEM facilities LEC, ROBOLAB, LBE, LPP, and RMN from LNBio, and UVX/MX2 beamline from LNLS.

■ REFERENCES

(1) Loeber, G., Dworkin, M. B., Infante, A., and Ahorn, H. (1994) Characterization of Cytosolic Malic Enzyme in Human Tumor Cells. *FEBS Lett. 344* (2−3), 181−186.

(2) Loeber, G., Maurer-Fogy, I., and Schwendenwein, R. (1994) Purification, CDNA Cloning and Heterologous Expression of the Human Mitochondrial NADP+-Dependent Malic Enzyme. *Biochem. J. 304* (3), 687−692.

(3) Loeber, G., Infante, A. A., Maurer-Fogy, I., Krystek, E., and Dworkin, M. B. (1991) Human NAD+-Dependent Mitochondrial Malic Enzyme: CDNA Cloning, Primary Structure, and Expression in Escherichia Coli. *J. Biol. Chem. 266* (5), 3016−3021.

(4) Takeo, K., Murai, T., Nagai, J., and Katsuki, H. (1967) Allosteric Activation of DPN-Linked Malic Enzyme from Escherichia Coli by Aspartate. *Biochem. Biophys. Res. Commun. 29* (5), 717−722.

(5) Leroux, A. E., Maugeri, D. a, Opperdoes, F. R., Cazzulo, J. J., and Nowicki, C. (2011) Comparative Studies on the Biochemical Properties of the Malic Enzymes from Trypanosoma Cruzi and Trypanosoma Brucei. *FEMS Microbiol. Lett. 314* (1), 25−33.

(6) Giordana, L., Sosa, M. H., Leroux, A. E., Mendoza, E. F. R., Petray, P., and Nowicki, C. (2018) Molecular and Functional Characterization of Two Malic Enzymes from Leishmania Parasites. *Mol. Biochem. Parasitol. 219*, 67.

(7) Karsten, W. E., Pais, J. E., Jagannatha Rao, G. S., Harris, B. G., and Cook, P. F. (2003) Ascaris Suum NAD-Malic Enzyme Is Activated by L-Malate and Fumarate Binding to Separate Allosteric Sites. *Biochemistry 42* (32), 9712−9721.

(8) Grissom, C. B., Canellas, P. F., and Wedding, R. T. (1983) Allosteric Regulation of the NAD Malic Enzyme from Cauliflower: Activation by Fumarate and Coenzyme A. *Arch. Biochem. Biophys. 220* (1), 133−144.

(9) Dey, P., Baddour, J., Muller, F., Wu, C. C., Wang, H., Liao, W. T., Lan, Z., Chen, A., Gutschner, T., Kang, Y., Fleming, J., Satani, N., Zhao, D., Achreja, A., Yang, L., Lee, J., Chang, E., Genovese, G., Viale, A., Ying, H., Draetta, G., Maitra, A., Wang, Y. A., Nagrath, D., and Depinho, R. A. (2017) Genomic Deletion of Malic Enzyme 2 Confers Collateral Lethality in Pancreatic Cancer. *Nature 542* (7639), 119−123.

(10) Sauer, L. A. (1973) Mitochondrial NAD-Dependent Malic Enzyme: A New Regulatory Enzyme. *FEBS Lett. 33* (2), 251−255.

(11) Hsieh, J. Y., Li, S. Y., Chen, M. C., Yang, P. C., Chen, H. Y., Chan, N. L., Liu, J. H., and Hung, H. C. (2014) Structural Characteristics of the Nonallosteric Human Cytosolic Malic Enzyme. *Biochim. Biophys. Acta, Proteins Proteomics 1844* (10), 1773−1783.

(12) Yang, Z., Zhang, H., Hung, H.-C., Kuo, C.-C., Tsai, L.-C., Yuan, H. S., Chou, W.-Y., Chang, G.-G., and Tong, L. (2002) Structural Studies of the Pigeon Cytosolic NADP(+)-Dependent Malic Enzyme. *Protein Sci. 11* (2), 332−341.

(13) Yang, Z., Floyd, D. L., Loeber, G., and Tong, L. (2000) Structure of a Closed Form of Human Malic Enzyme and Implications for Catalytic Mechanism. *Nat. Struct. Biol. 7* (3), 251−257.

(14) Xu, Y., Bhargava, G., Wu, H., Loeber, G., and Tong, L. (1999) Crystal Structure of Human Mitochondrial NAD(P)+-Dependent Malic Enzyme: A New Class of Oxidative Decarboxylases. *Structure 7* (8), 877−889.

(15) Tao, X., Yang, Z., and Tong, L. (2003) Crystal Structures of Substrate Complexes of Malic Enzyme and Insights into the Catalytic Mechanism. *Structure 11* (9), 1141−1150.

(16) Chang, G. G., and Tong, L. (2003) Structure and Function of Malic Enzymes, A New Class of Oxidative Decarboxylases. *Biochemistry 42*, 12721.

(17) Ranzani, A. T., Nowicki, C., Wilkinson, S. R., and Cordeiro, A. T. (2017) Identification of Specific Inhibitors of Trypanosoma Cruzi Malic Enzyme Isoforms by Target-Based HTS. *SLAS Discovery 22* (9), 1150−1161.

(18) Peña, I., Pilar Manzano, M., Cantizani, J., Kessler, A., Alonso-Padilla, J., Bardera, A. I., Alvarez, E., Colmenarejo, G., Cotillo, I., Roquero, I., De Dios-Anton, F., Barroso, V., Rodriguez, A., Gray, D. W., Navarro, M., Kumar, V., Sherstnev, A., Drewry, D. H., Brown, J. R., Fiandor, J. M., and Julio Martin, J. (2015) New Compound Sets Identified from High Throughput Phenotypic Screening against Three Kinetoplastid Parasites: An Open Resource. *Sci. Rep. 5* (8771), 8771.

(19) De Rycker, M., Baragaña, B., Duce, S. L., and Gilbert, I. H. (2018) Challenges and Recent Progress in Drug Discovery for Tropical Diseases. *Nature 559* (7715), 498−506.
(20) Zheng, W., Thorne, N., and McKew, J. C. (2013) Phenotypic Screens as a Renewed Approach for Drug Discovery. *Drug Discovery Today 18* (21−22), 1067−1073.
(21) Sykes, M. L., and Avery, V. M. (2013) Approaches to Protozoan Drug Discovery: Phenotypic Screening. *J. Med. Chem. 56* (20), 7727−7740.
(22) Moffat, J. G., Vincent, F., Lee, J. A., Eder, J., and Prunotto, M. (2017) Opportunities and Challenges in Phenotypic Drug Discovery: An Industry Perspective. *Nat. Rev. Drug Discovery 16* (8), 531−543.
(23) Eder, J., Sedrani, R., and Wiesmann, C. (2014) The Discovery of First-in-Class Drugs: Origins and Evolution. *Nat. Rev. Drug Discovery 13* (8), 577−587.
(24) Mondal, D. K., Pal, D. S., Abbasi, M., and Datta, R. (2021) Functional Partnership between Carbonic Anhydrase and Malic Enzyme in Promoting Gluconeogenesis in Leishmania Major. *FEBS J.*, 4129−4152.
(25) Shiratsubaki, I. S., Fang, X., Souza, R. O. O., Palsson, B. O., Silber, A. M., and Siqueira-Neto, J. L. (2020) Genome-Scale Metabolic Models Highlight Stage-Specific Differences in Essential Metabolic Pathways in Trypanosoma Cruzi. *PLoS Neglected Trop. Dis. 14* (10), No. e0008728.
(26) Yang, Z., Lanks, C. W., and Tong, L. (2002) Molecular Mechanism for the Regulation of Human Mitochondrial NAD(P)+-Dependent Malic Enzyme by ATP and Fumarate. *Structure 10* (7), 951−960.
(27) Yang, Z., Batra, R., Floyd, D. L., Hung, H. C., Chang, G. G., and Tong, L. (2000) Potent and Competitive Inhibition of Malic Enzymes by Lanthanide Ions. *Biochem. Biophys. Res. Commun. 274* (2), 440−444.
(28) Alvarez, C. E., Bovdilova, A., Höppner, A., Wolff, C. C., Saigo, M., Trajtenberg, F., Zhang, T., Buschiazzo, A., Nagel-Steger, L., Drincovich, M. F., Lercher, M. J., and Maurino, V. G. (2019) Molecular Adaptations of NADP-Malic Enzyme for Its Function in C4 Photosynthesis in Grasses. *Nat. Plants 5* (7), 755−765.
(29) Coleman, D. E., Rao, G. S. J., Goldsmith, E. J., Cook, P. F., and Harris, B. G. (2002) Crystal Structure of the Malic Enzyme from Ascaris Suum Complexed with Nicotinamide Adenine Dinucleotide at 2.3 Å Resolution. *Biochemistry 41* (22), 6928−6938.
(30) Rao, G. S. J., Coleman, D. E., Karsten, W. E., Cook, P. F., and Harris, B. G. (2003) Crystallographic Studies on Ascaris Suum NAD-Malic Enzyme Bound to Reduced Cofactor and Identification of an Effector Site. *J. Biol. Chem. 278* (39), 38051−38058.
(31) Burley, K. H., Cuthbert, B. J., Basu, P., Newcombe, J., Irimpan, E. M., Quechol, R., Foik, I. P., Mobley, D. L., Beste, D. J. V., and Goulding, C. W. (2021) Structural and Molecular Dynamics of Mycobacterium Tuberculosis Malic Enzyme, a Potential Anti-TB Drug Target. *ACS Infect. Dis. 7* (1), 174−188.
(32) Avilán, L., and Garcia, P. (1994) Hysteresis of Cytosolic NADP-Malic Enzyme II from Trypanosoma Cruzi. *Mol. Biochem. Parasitol. 65* (2), 225−232.
(33) Cazzulo, J. J., Juan, S. M., and Segura, E. L. (1977) The Malic Enzyme from Trypanosoma Cruzi. *J. Gen. Microbiol. 99* (1), 237−241.
(34) Krissinel, E., and Henrick, K. (2007) Inference of Macromolecular Assemblies from Crystalline State. *J. Mol. Biol. 372* (3), 774−797.
(35) Hsieh, J. Y., Li, S. Y., Tsai, W. C., Liu, J. H., Lin, C. L., Liu, G. Y., and Hung, H. C. (2015) A Small-Molecule Inhibitor Suppresses the Tumor-Associated Mitochondrial NAD(P)+-Dependent Malic Enzyme (ME2) and Induces Cellular Senescence. *Oncotarget 6* (24), 20084−20098.
(36) Hsieh, J. Y., Liu, J. H., Yang, P. C., Lin, C. L., Liu, G. Y., and Hung, H. C. (2014) Fumarate Analogs Act as Allosteric Inhibitors of the Human Mitochondrial NAD(P)+-Dependent Malic Enzyme. *PLoS One 9* (6), No. e98385.
(37) Sander, T., Freyss, J., Von Korff, M., and Rufener, C. (2015) DataWarrior: An Open-Source Program for Chemistry Aware Data Visualization and Analysis. *J. Chem. Inf. Model. 55* (2), 460−473.
(38) Wilcken, R., Zimmermann, M. O., Lange, A., Joerger, A. C., and Boeckler, F. M. (2013) Principles and Applications of Halogen Bonding in Medicinal Chemistry and Chemical Biology. *J. Med. Chem. 56*, 1363.
(39) Sánchez-Valdéz, F. J., Padilla, A., Wang, W., Orr, D., and Tarleton, R. L. (2018) Spontaneous Dormancy Protects Trypanosoma Cruzi during Extended Drug Exposure. *eLife 7*, No. e34039.
(40) Mercaldi, G. F., Ranzani, A. T., and Cordeiro, A. T. (2014) Discovery of New Uncompetitive Inhibitors of Glucose-6-Phosphate Dehydrogenase. *J. Biomol. Screening 19* (10), 1362−1371.
(41) Davis, M. I., Shen, M., Simeonov, A., and Hall, M. D. (2016) Diaphorase Coupling Protocols for Red-Shifting Dehydrogenase Assays. *Assay Drug Dev. Technol. 14* (3), 207−212.
(42) Kabsch, W. (2010) XDS. *Acta Crystallogr., Sect. D: Biol. Crystallogr. 66* (2), 125−132.
(43) Winn, M. D., Ballard, C. C., Cowtan, K. D., Dodson, E. J., Emsley, P., Evans, P. R., Keegan, R. M., Krissinel, E. B., Leslie, A. G. W., McCoy, A., McNicholas, S. J., Murshudov, G. N., Pannu, N. S., Potterton, E. A., Powell, H. R., Read, R. J., Vagin, A., and Wilson, K. S. (2011) Overview of the CCP4 Suite and Current Developments. *Acta Crystallogr., Sect. D: Biol. Crystallogr. 67*, 235−242.
(44) Evans, P. R., and Murshudov, G. N. (2013) How Good Are My Data and What Is the Resolution? *Acta Crystallogr., Sect. D: Biol. Crystallogr. 69* (Pt 7), 1204−1214.
(45) McCoy, A. J., Grosse-Kunstleve, R. W., Adams, P. D., Winn, M. D., Storoni, L. C., and Read, R. J. (2007) Phaser Crystallographic Software. *J. Appl. Crystallogr. 40* (4), 658−674.
(46) Afonine, P. V., Grosse-Kunstleve, R. W., Echols, N., Headd, J. J., Moriarty, N. W., Mustyakimov, M., Terwilliger, T. C., Urzhumtsev, A., Zwart, P. H., and Adams, P. D. (2012) Towards Automated Crystallographic Structure Refinement with Phenix.Refine. *Acta Crystallogr., Sect. D: Biol. Crystallogr. 68* (4), 352−367.
(47) Murshudov, G. N., Skubák, P., Lebedev, A. A., Pannu, N. S., Steiner, R. a., Nicholls, R. A., Winn, M. D., Long, F., and Vagin, A. A. (2011) REFMAC5 for the Refinement of Macromolecular Crystal Structures. *Acta Crystallogr., Sect. D: Biol. Crystallogr. 67* (4), 355−367.
(48) Emsley, P., Lohkamp, B., Scott, W. G., and Cowtan, K. (2010) Features and Development of Coot. *Acta Crystallogr., Sect. D: Biol. Crystallogr. 66* (Pt 4), 486−501.
(49) Yang, H., Guranovic, V., Dutta, S., Feng, Z., Berman, H. M., and Westbrook, J. D. (2004) Automated and Accurate Deposition of Structures Solved by X-Ray Diffraction to the Protein Data Bank. *Acta Crystallogr., Sect. D: Biol. Crystallogr. 60* (10), 1833−1839.
(50) Fredo Naciuk, F., Do Nascimento Faria, J., Gonçalves Eufrásio, A., Torres Cordeiro, A., and Bruder, M. (2020) Development of Selective Steroid Inhibitors for the Glucose-6-Phosphate Dehydrogenase from Trypanosoma Cruzi. *ACS Med. Chem. Lett. 11* (6), 1250−1256.
(51) Reverdin, F., and de Luc, A. (1912) Nitrierung Der Acylderivate Des P-Anisidins. [Fortsetzung.]. *Ber. Dtsch. Chem. Ges. 45*, 349−354.
(52) Baraldi, P. G., Moorman, A. R., and Borea, P. A. Novel Adenosine A3 Receptor Agonists. WO2005028489A2, March 31, 2005.

https://doi.org/10.1021/acsinfecdis.1c00231
ACS Infect. Dis. XXXX, XXX, XXX−XXX